

Strike-slip Enables Subduction Initiation beneath a Failed Rift: New Seismic Constraints from Puysegur Margin, New Zealand

Brandon Shuck^{1,2}, Harm Van Avendonk¹, Sean P. S. Gulick^{1,2}, Michael Gurnis³, Rupert Sutherland⁴, Joann Stock³, Jiten Patel⁴, Erin Hightower³, Steffen Saustrop¹, Thomas Hess^{1,2}

¹Institute for Geophysics, Jackson School of Geosciences, University of Texas at Austin, Austin, TX 78758, USA.

²Department of Geological Sciences, Jackson School of Geosciences, University of Texas at Austin, Austin, TX 78712, USA

³Seismological Laboratory, California Institute of Technology, Pasadena, CA 91125, USA.

⁴School of Geography, Environment and Earth Sciences, Victoria University of Wellington, Wellington 6140, New Zealand.

Corresponding author: Brandon Shuck (brandon.shuck@utexas.edu)

Key Points:

- Deep-penetrating seismic velocity and reflection images provide constraints on regional crustal structure of an incipient subduction zone
- Earlier phases of continental rifting, seafloor spreading, and strike-slip produced weaknesses that facilitated subduction initiation
- Subduction nucleated at a restraining bend as ~10 Myr thin and dense oceanic lithosphere underthrust buoyant continental lithosphere

Abstract

Subduction initiation often takes advantage of previously weakened lithosphere and may preferentially nucleate along pre-existing plate boundaries. To evaluate how past tectonic regimes and inherited lithospheric structure might lead to self-sustaining subduction, we present an analysis of the Puysegur Trench, a young subduction zone with a rapidly evolving tectonic history. The Puysegur margin, south of New Zealand, has experienced a transformation from rifting to seafloor spreading to strike-slip, and most recently to incipient subduction, all in the last ~45 million years. Here we present deep-penetrating multichannel reflection (MCS) and ocean-bottom seismometer (OBS) tomographic images to document crustal structures along the margin. Our images reveal that the overriding Pacific Plate beneath the Solander Basin contains stretched continental crust with magmatic intrusions, which formed from Eocene-Oligocene rifting between the Campbell and Challenger plateaus. Rifting was more advanced to the south, yet never proceeded to breakup and seafloor spreading in the Solander Basin as previously thought. Subsequent strike-slip deformation translated continental crust northward causing an oblique collisional zone, with trailing ~10 Myr old oceanic lithosphere. Incipient subduction transpired as oceanic lithosphere from the south forcibly underthrust the continent-collision zone. We suggest that subduction initiation at the Puysegur Trench was assisted by inherited buoyancy contrasts and structural weaknesses that were imprinted into the lithosphere during earlier phases of continental rifting and strike-slip along the plate boundary. The Puysegur margin demonstrates that forced nucleation along a strike-slip boundary is a viable subduction initiation scenario and should be considered throughout Earth's history.

Plain Language Summary

Subduction zones, where one plate underthrusts another, are the principal driver of tectonic plate motions on Earth; however, the origin of these convergent margins remains unsolved. Geoscientists have proposed that the process of forming a new subduction zone takes advantage of weaknesses such as buoyancy contrasts and re-using older weak plate boundaries. To test these ideas, we use new seismic images to document tectonic structures at the Puysegur margin, an incipient subduction zone south of New Zealand. Our images reveal that the upper plate of the Puysegur margin consists mostly of stretched continental lithosphere that formed during an Eocene-Oligocene extension phase. Following extension, a translational phase juxtaposed thin and high-density oceanic lithosphere against thick and low-density continental lithosphere in a wide damage zone. Convergence across this zone led to underthrusting of the Australian Plate beneath the Pacific Plate and the development of the newly established Puysegur subduction zone. Our results demonstrate that subduction initiation was aided by lithospheric buoyancy contrasts and weak zones inherited from earlier phases of tectonic activity. Our findings argue that pre-existing plate boundaries, weakening mechanisms, and strike-slip are key components of the subduction initiation process and have likely prevailed throughout Earth's history.

1. Introduction

Tracing the evolution of plate boundaries and their response to variations in the state of stress through time is fundamental to understanding global tectonics. The degree to which these lithospheric plates are actively driving thermal convection of the deeper mantle, or vice versa, is still debated (Bercovici et al., 2003; Coltice et al., 2019; Ghosh & Holt, 2012). Plate reconstructions suggest that collisional, extensional, and translational styles of movement along long-lived and relatively weak plate boundaries (Carpenter et al., 2011; Karato & Barbot, 2018; Lachenbruch & Sachs, 1980; Sutherland et al., 2017; Vissers et al., 1991; Zhong & Gurnis, 1996) have facilitated the evolution of continental and oceanic plates in Earth's post-Archean history (Li et al., 2008; Müller et al., 2019). For example, Wilson (1966) recognized that oceanic domains appeared to be closing and then later re-opening along ancient mountain belts. Large strike-slip offsets are also a common element of this global tectonic cycle and potentially key to evolution of plate configurations (Dalziel & Dewey, 2019). Although there is a rich record of the geological processes associated with continental rifting and the onset of seafloor spreading (Osmundsen & Ebbing, 2008; Shillington et al., 2008; White et al., 2008; Rooney et al., 2014; Shuck et al., 2019), there are fewer observational constraints on the initiation of subduction zones (Gurnis et al., 2004; Stern & Gerya, 2018) because the convergent margins are not well preserved in the rock record.

Subduction zones, where oceanic lithosphere is recycled into the deep mantle, may be the most critical component of the plate tectonic cycle, as geodynamic models suggest that the slab pull edge force is the main driver of plate movements (Forsyth & Uyeda, 1975; Lithgow-Bertelloni & Richards, 1995; Stadler et al., 2010). Although great progress has been made in describing the structure and stresses at mature subduction zones (e.g., Abers et al 2006; Bangs et al., 2004; Stern, 2002), the process of subduction zone initiation (SZI) is not well understood and remains one of the last major unsolved problems in plate tectonics (Gurnis et al., 2004; Stern and Gerya, 2018; Chotalia et al., 2020). There is not a unique tectonic setting in which subduction is thought to begin; however, there is general agreement that it requires the exploitation of lithospheric weaknesses and may preferentially nucleate along pre-existing plate boundaries (McKenzie, 1977; Stern & Gerya, 2018; Toth & Gurnis, 1998). Proposed settings for SZI include nucleation along

an old fracture zone (e.g., Izu-Bonin-Mariana Trench), an extinct mid-ocean ridge and/or transform fault (e.g., South Scotia), an extinct volcanic arc complex (e.g., Tonga-Kermadec Trench), polarity reversal behind an active subduction zone (e.g., New Hebrides), or on the flanks of a large igneous province (e.g., Caribbean) (Gurnis et al., 2004; Stern & Gerya, 2018).

The wide variety of tectonic settings for SZI has caused substantial debate about the forces and critical geodynamic ingredients necessary to drive this process. Two distinct categories of SZI have been proposed (Chotalia et al., 2020): horizontally forced (c.f., Gurnis et al., 2004) versus vertically forced (c.f., Stern, 2004). Horizontally forced SZI is a response to tectonic stresses and continuing plate convergence, which may be externally forced over large distances. Vertically forced SZI is driven by a local, catastrophic gravitational instability in oceanic lithosphere, causing the plate to fail and collapse downwards. Geodynamic models predict horizontally forced SZI would be accompanied by compression and uplift of the overriding plate (Gurnis et al., 2004), whereas vertically forced SZI would produce only extension in the upper plate. Unfortunately, the geological record generally lacks clear evidence as to whether a mature subduction zone may have formed by gravitational collapse or if far-field stresses were involved, because the evidence of early subduction is often overprinted by intense deformation and arc volcanism. Thus, field observations of an incipient subduction zone are necessary to test model predictions of stress states, vertical tectonics, and the role of weakening mechanisms during the subduction initiation process.

In this paper, we detail geophysical observations and analyze an incipient subduction zone suggested to be the best modern example of horizontally forced SZI. We focus on the Puysegur Trench, located south of New Zealand (Figure 1), where the margin has evolved from rifting, to strike-slip, to incipient subduction since the Eocene (e.g., Lebrun et al., 2003). The Puysegur margin is a unique location to investigate processes associated with subduction initiation, since there is a significant amount of plate convergence, the past plate motion is well constrained, and the geologic record is not overprinted (e.g., Gurnis et al., 2004). Here, we present a seismic structural analysis from the first regional seismic survey of the Puysegur margin. We use high-quality seismic images to document structures related to older extension and younger convergent deformation to examine whether subduction may initiate by taking advantage of structural weaknesses that were created during earlier tectonic phases.

2. Tectonic Setting and Evolution of Zealandia

2.1 Continental crust of New Zealand

The continental crust of New Zealand is comprised of distinct tectonostratigraphic terranes and igneous suites that were either part of Paleozoic Gondwana or sediments and crustal fragments that accreted westward onto the margin of eastern Gondwana (e.g., Bishop et al., 1985; Cox & Sutherland, 2007). These basement terranes have been grouped into the Western and Eastern provinces, separated by the massive subduction-related Median Batholith (Mortimer et al., 1999; Figure 1). The Western Province, which is exposed in Westland and Fiordland, consists of the Buller Terrane and the Takaka Terrane. The Buller Terrane is composed of Late Cambrian to Late Ordovician quartzite, whereas the Takaka Terrane contains a range of highly deformed Paleozoic sedimentary and volcanic rocks; both terranes are intruded by various batholiths (Nathan, 1976; Cooper, 1989). The younger Eastern Province (Permian to Cretaceous) is dominated by lithic and feldspathic metamorphosed graywackes but also includes volcanic, intrusive, and ophiolite domains (Bishop, 1985). Offshore, Cretaceous schists, granites and granodiorites recovered south of New Zealand on island outcrops, from seafloor dredges, and petroleum boreholes share characteristics with exposures on South Island (Mortimer et al., 2017; Scott et al., 2015). Onshore

terrane boundaries may therefore extend offshore (e.g., Beggs et al., 1990), which suggests the Campbell Plateau basement is similar to Paleozoic rocks of the Western Province.

The Cretaceous marked the beginning of major plate reorganizations in the southwest Pacific. The convergent margin of eastern Gondwana transitioned to widespread rifting and volcanism between 110-85 Ma (Bradshaw, 1989; Tulloch et al., 2009). New rift zones in eastern Gondwana filled with volcanic and marine deposits (Laird & Bradshaw, 2004; Riefstahl et al., 2020) at this time. Sustained extension eventually culminated in the successful breakup of this part of Gondwana around ~83 Ma and subsequent seafloor spreading in the Tasman and Southwest Pacific basins, effectively separating the continents of Australia, Antarctica, and Zealandia (Bache et al., 2014; Mortimer et al., 2017).

2.2 Cenozoic evolution

Seafloor spreading at Tasman Ridge separated Australia and Zealandia until ~53 Ma (Gaina et al., 1998), when the nucleation of new subduction zones in the southwest Pacific caused a far-field shift in plate motions (Sutherland et al., 2020). The death of the Tasman Ridge, combined with faster spreading between Australia and Antarctica, sparked the development of a new Australian-Pacific plate boundary (AUS-PAC) in the middle Eocene, oriented nearly orthogonal to the Cretaceous Tasman Ridge, which now lies northwest of New Zealand (Wood et al., 1996; Cande & Stock, 2004). At approximately ~45 Ma, intraoceanic rifting formed the Macquarie Spreading Center (MSC), which separated the conjugate rifted margins of the Resolution Ridge System on the Australian Plate and the southwestern Campbell Plateau on the Pacific Plate (Sutherland, 1995). It is thought that orthogonal and symmetric seafloor spreading along the MSC extended to at least ~47.5°S into the Solander Trough, and that farther north marked a transition to distributed normal faulting within continental crust producing the Solander Basin (Sutherland & Melhuish, 2000; Lebrun et al., 2003).

Starting around ~30 Ma, the AUS-PAC stage pole of plate motion migrated southeast relative to the Pacific plate, resulting in progressively more oblique seafloor spreading along the MSC (Cande & Stock, 2004; Keller, 2004). Consequently, the MSC transitioned into short, oblique spreading segments separated by long offset fracture zones, which curved through time (Lamarche et al., 1997). Sustained changes in plate motions caused fracture zones to eventually link and form the Macquarie Ridge Complex (MRC) with dominantly dextral strike-slip by ~25 Ma (e.g., Keller, 2004). Coeval with the establishment of the MRC, the Alpine Fault to the north formed a major strike-slip boundary west of Fiordland, offsetting the Median Batholith and adjacent terranes of New Zealand (Kamp, 1986; Sutherland et al., 2000; Figure 1). The Alpine Fault and MRC were connected by a transpressive relay zone at Puysegur Bank, located proximally offshore southern Fiordland, evidenced by the migration of faults in a left-stepping manner and thrust faulting causing uplift and erosion of Eocene-Miocene stratigraphy (Lamarche & Lebrun, 2000, Sutherland et al., 2006).

The timing and geodynamic conditions of subduction initiation at the Puysegur margin are poorly understood due to a lack of high-quality geophysical data and ocean drilling throughout the region. Collot et al. (1995) suggested that subduction initiated along an oceanic fracture zone around ~10 Ma, which gradually weakened and reoriented to facilitate underthrusting. Alternatively, Lebrun et al. (2003) argues that subduction initiated near Puysegur Bank around ~20 Ma and involved the underthrusting of Solander Trough's conjugate oceanic lithosphere beneath the transpressive continental relay zone. It is also possible that the subduction front retreated westward behind a fracture zone, stranding a sliver of oceanic lithosphere between

Puysegur Trench and Puysegur Ridge (Collot et al., 1995; Lebrun et al., 2003; Sutherland et al., 2006). Sutherland et al. (2006) used the geometry of the Benioff zone beneath Fiordland to estimate the timing of subduction initiation between ~16-10 Ma for subduction beneath Fiordland and ~6 Ma for the southern Puysegur Trench, reflecting a southward propagation over time.

2.3 Modern plate boundary

Puysegur Trench and Ridge comprise the northern extension of the Macquarie Ridge Complex (MRC), which forms the Australian-Pacific (AUS-PAC) plate boundary, extending over 2200 km from the Alpine Fault of New Zealand's South Island to the Australia-Pacific-Antarctic triple junction (Figure 1, 2). The tectonic segmentation and structure of the MRC is likely a consequence of the transition in AUS-PAC plate motion from divergence to strike-slip throughout the Cenozoic (Massell et al., 2000; Lebrun et al., 2003; Cande & Stock, 2004). From south to north these segments are the Hjort, Macquarie, McDougall, and Puysegur sections of the plate boundary (Figure 1). All of the MRC segments exhibit uplifted ridges formed by transpression (Massell et al., 2000). Owing to a greater component of convergence through time, the Hjort Trench shows evidence of underthrusting (Meckel et al., 2003), whereas the Puysegur segment is in the process of developing into a mature subduction zone (Lebrun et al., 2003; Gurnis et al., 2019; Sutherland et al., 2006). Conversely, the central Macquarie and McDougall segments exhibit little to no evidence for underthrusting and earthquake focal mechanisms indicate primarily dextral strike-slip movement (Frohlich et al., 1997; Massell et al., 2000).

The Puysegur Margin exhibits several characteristics of a subduction zone: a deep (>6 km) ocean trench, a seismically active Benioff zone to ~150 km depth beneath Fiordland (Eberhart-Philips & Reyners, 2001), and young, adakitic volcanism on the overriding plate close to South Island (Mortimer et al., 2013). Presently, the Australian Plate is converging obliquely with the Pacific Plate at a rate of ~37 mm/yr (MORVEL, DeMets et al., 2010). This plate motion is partitioned between the Puysegur Trench and adjacent strike-slip Puysegur Fault to the east (Hayes et al., 2009; Figure 2). Seismicity data outline the subducting Australian slab as an inverted "ploughshare" shape that sharply twists to nearly vertical beneath Fiordland in the southwestern corner of South Island (Christoffel & van der Linden, 1972; Eberhart-Philips & Reyners, 2001).

The upper plate of the Puysegur subduction zone, which is formally part of the Pacific Plate, has been divided into the Eocene-Miocene oceanic Solander Basin, which transitions northward to the continental Solander Basin near ~47.5°S, both of which are bounded to the west by Puysegur Ridge and to the east by the continental Campbell Plateau (Sutherland and Melhuish, 2000; Lebrun et al., 2003; Figure 1, 2). Previous studies have classified the northern Puysegur margin as an oceanic-under-continental subduction zone, but south of ~47.5°S as an intra-oceanic subduction zone (Collot et al., 1995; Massell et al., 2000; Sutherland and Melhuish, 2000; Lebrun et al., 2003). In the north, morphology of Puysegur Ridge is flat-topped, wide, and resides at ~1500 m water depth, and the adjacent Snares Zone exhibits a strong negative gravity anomaly, which are all used as evidence that the upper plate has subsided, possibly in response to the slab becoming more negatively buoyant (Figure 2; Collot et al., 1995; Gurnis et al., 2004). In contrast, towards the south the Puysegur Ridge is narrow, steep-sided, shallower, and the trench terminates against Puysegur Ridge near the junction with the McDougall segment to the south, leading to the interpretation that subduction along the southern Puysegur Trench is still in an incipient phase (Collot et al., 1995; Delteil et al., 1996). Understanding these along-strike variations requires a detailed tectonic framework for the timing and location of subduction initiation, as well as details of the physical and structural properties of the lithosphere involved.

3. Data Acquisition, Processing, and Analysis

In February and March 2018, the South Island Subduction Initiation Experiment (SISIE) imaged the structure of the Australian and Pacific plates to better understand the regional tectonic evolution and subduction initiation at the Puysegur margin. Using the R/V *Marcus Langseth*, the shipboard party collected multichannel seismic (MCS), ocean-bottom seismometer (OBS), multi-beam bathymetry, and other geophysical data across the Puysegur margin (see Text S1). In total, 1252 km of MCS data were acquired on seven 2D lines, two of which were coincident with OBS deployments (Figure 2). The SISIE dataset comprises the first regional, high-fold, and deep-penetrating MCS and OBS seismic coverage of the Puysegur margin.

We interpret five distinct wide-angle seismic phases, including refractions and reflections, from OBS records along transects SISIE-1 and SISIE-2, which traverse the incoming oceanic plate, Puysegur Trench, Puysegur Ridge, Solander Basin, and onto the Campbell Plateau (Figure 2, 3). Travel times for the basement reflection from coincident MCS data along SISIE-1 and SISIE-2 were also incorporated into layered models. We performed a tomographic inversion of all travel-time data to simultaneously constrain layer thickness and seismic velocities on each of the transects (Text S3). The product of the iterative inversion process yields a smooth characterization of the subsurface velocity structure, including velocity discontinuities across the top of basement and Moho interfaces. We tested the recovery of a 12 km horizontal by 6 km vertical perturbation ellipse (Text S3) to test the robustness of our tomographic images (Figure 4). Our final preferred compressional-wave (V_p) velocity models along SISIE-1 and SISIE-2 are integrated with MCS images to jointly interpret crustal structure along the margin.

Seismic processing of the SISIE MCS data utilized conventional crustal imaging techniques. Specific parameters of our workflow are described in the supporting information (Text S4). Seismic processing involved trace editing, noise suppression, geometry assignment, velocity analysis, multiple suppression, band-pass frequency filtering, and corrective trace dip filtering. Seismic velocity models for Kirchhoff pre-stack depth migration algorithms were derived from the smoothed RMS stacking velocities. For the SISIE-1 and SISIE-2 lines coincident with OBS data, a merged velocity section with MCS-derived velocities for shallow sediments and OBS-derived velocities for crust and mantle structure produced the best images. The result of our processing workflow yields seven pre-stack depth migrated (PSDM) lines across the Puysegur margin.

4. Results and Interpretations of SISIE Seismic Profiles

Gurnis et al. (2019) showed preliminary time-migrated seismic images along the Puysegur Margin from the SISIE experiment. Here we present more advanced pre-stack depth-migrated seismic images that further elucidate the regional tectonic structure of the margin. We integrate our tectonic interpretation with results from Patel et al. (2020), who used SISIE MCS images to interpret the depositional history of Solander Basin stratigraphy and create a spatially and temporally consistent framework tied to biostratigraphic ages from the Parara-1 petroleum well. The seismic horizons and nomenclature used in this study correspond to the top of the units defined by Patel et al. (2020).

4.1 SISIE-1 – Southern Regional Dip Line

SISIE-1 is a 206 km-long line oriented west-east at $\sim 49.5^\circ\text{S}$, of which ~ 180 km of MCS and corresponding OBS tomography images and shipboard bathymetry are shown in Figure 5. This profile is oriented subparallel to the abyssal hill fabric of the slow-spread oceanic lithosphere of the incoming Australian plate. Our seismic image shows a rough basement reflection which periodically crops out at the seafloor but is otherwise buried by small isolated pockets of sediments

typically less than a few hundred meters thick. We find minimal discernable seismic structure beneath the basement, possibly overshadowed by seismic artefacts arising from out-of-plane seafloor reflections and diffractions from the rough seafloor, or due to the complex internal structure of the slow-spread oceanic crust. In contrast, clear Moho reflections are observed on the OBS data records and our final tomographic image suggests that the oceanic crust (between the basement and Moho) of the incoming Australian plate is 5-6 km thick and the seismic velocity structure is as expected for oceanic crust of this age and spreading rate (Figure 5).

Near CMP 26250, SISIE-1 orthogonally crosses the L'Atalante Fracture Zone where we observe a broad basement high with ~1 km of vertical relief over a lateral distance of ~10 km. Trenchward of the fracture zone, the seafloor and basement slope steepen dip to ~5°, the overlying sedimentary cover thickens to ~500 m, and several normal faults offset the sedimentary column and top of crust. The trench-parallel orientation of these normal faults is clearly visible on shipboard multibeam bathymetry (Figure 5c). At CMP ~23500 a significant east-dipping normal fault is imaged offsetting the basement by ~1.2 km, and the highly fractured basement geometry continues downdip and eastward where it becomes buried under trench-fill sediments. In the upper crust, several highly reflective sedimentary zones are flanked by basement highs (Figure 5a). Below the crust, the upper mantle Vp decreases laterally from ~7.7 to ~7.1 km/s (Figure 5e).

At the trench (CMP ~22850), ~700 m thick sedimentary cover overlies the Australian basement as it underthrusts the Pacific Plate. A bright, continuous, and negative polarity reflection dipping at ~9° above the subducting plate extends for ~20 km landward of the trench until it is overprinted by strong water-bottom multiples. Above this reflection, a zone of gently folded sediments extends ~5 km east of the trench and coincides with a low Vp of ~2.5 km/s. From CMP ~22000-19000, a ~400 m thick layer of sediments parallel to the seafloor is imaged along the steep (~10°) inner-trench slope. Beneath this thin layer, the internal upper plate basement is seismically opaque. Here, the upper-plate basement velocities with depth increase quickly from ~4 km/s to ~6 km/s, and the crust thickens eastward to ~12 km at the western flank of Puysegur Ridge. Atop Puysegur Ridge, an axial valley separates two flanks with more than 1.5 km of vertical relief, all of which appears to be sediment-free; thus basement rock crops out along the seafloor.

We interpret the bright and negative polarity reflection as the décollement, marking the interface between the underthrusting and overriding plates (Figure 5a). This interpretation also implies the folded sediments were accreted to the upper plate, either by frontal accretion or underplating.

No faults were imaged beneath Puysegur Ridge, although earthquake focal mechanisms suggest that a major component of strike-slip faulting occurs near the axial valley (Figure 2). Our tomographic image reveals a relatively sharp increase in mid-lower crustal Vp laterally across the axial valley (Figure 5e).

SISIE-1 presents an unprecedented view of the Solander Basin crustal structure and stratigraphy. Crustal thickness decreases from ~12 km at the eastern flank of Puysegur Ridge to just ~6 km at the eastern edge of the basin (Figure 5e). The top of crust is offset by numerous normal faults that are imaged deep into the lower crust, forming rotated crustal blocks in horst-graben structures (Figure 5d). The seismic character of the uppermost crust is variable throughout the basin. For instance, atop a horst structure between CMP ~4750-5750, we observe a sharp transition from the overlying sediments to underlying crystalline crustal rocks marked by high-amplitude and continuous reflectivity. In contrast, throughout much of the basin we image a thin transition (100s of meters) from overlying strata to the top of basement, containing patches of discontinuous, high-amplitude, and chaotic reflectivity. In some locations (CMP ~8500), this

transition also contains pointed and serrated structures which are associated with folding, localized normal faulting, and seismic amplitude anomalies in the overlying sediments.

We interpret the lowermost coherent reflection of the transitional sequence as representing the top of crystalline basement (black line in Figure 5). We suggest that this layer in the upper crust is volcanic in origin and refer to the upper boundary of this zone as the top of the volcanic layer (red line in Figure 5). The volcanic zone has variable structure and likely constitutes a combination of distributed extrusive flows (CMP ~3000), focused volcanic cones (CMP ~8350, 8500, and 8750), and intruded sediments and/or volcanoclastic deposits (CMP ~11500).

Seismic velocities sharply increase beneath the volcanic layer and top of basement to $V_p > \sim 5$ km/s. Within the mid-lower crust, we observe an assemblage of very high-amplitude and low frequency seismic reflections which originate ~2-7 km beneath the top of basement and are persistent throughout the basin (Figure 5b, 5d).

Intracrustal reflectivity of this nature could arise from either lower crust ductile shear zones (e.g., McIntosh et al., 2014), remnants of older brittle fault zones (e.g., McDermott & Reston, 2015), or magmatic intrusions (e.g., White et al., 2008). These bright regions overlie and coincide with zones of anomalously high V_p (> 7.1 km/s), which are commonly attributed to mafic intrusions and/or magmatic underplating (e.g., Holbrook et al., 1994). The coincidence of lower crustal reflectivity with high V_p strongly suggests igneous intrusions. Fault plane reflections show higher amplitudes near high-velocity lower crust (Figure 5b); thus, mantle-derived melts may have migrated along fault zones to feed volcanism in the upper crust.

Following the analyses of Patel et al. (2020), which interpreted stratigraphic units in the Solander Basin, we define three distinct tectonostratigraphic intervals based on their large-scale seismic reflection geometry and relationships to tectonic structures. The total sedimentary fill across the basin increases from west to east and reaches a maximum of ~3.5 km adjacent to the Campbell Plateau. The deepest stratigraphic package (top of volcanic layer to SLS1-1) exhibits prograde and divergent fill patterns contained in fault-bounded wedges that thicken towards and onlap the footwall of uplifted basement rocks (e.g., CMP ~6000), indicating that deposition was synchronous with tectonic extension. In some areas, these sediments are tightly folded above volcanic cones (CMP ~8500) and/or thin against volcanic highs, therefore deposition was coeval or slightly older than volcanism. From SLS1-1 to SLS2-4, the internal stratigraphy is mostly subparallel and has a nearly constant thickness across the basin, although some disruption from internal faulting and downlap is observed on the eastern edge (CMP ~2000-4750). Faults within this package are located above elevated basement topography (e.g., CMP ~4750, 5750) and volcanic cones (e.g., CMP ~8500). At the basin scale, the entire SLS1-1 to SLS2-4 sequence forms an open fold and broad anticline centered near CMP ~6000, which is also where the axis of the modern Solander Channel is located. Additionally, tectonostratigraphic packages bounded by top of volcanic layer to SLS1-1, and SLS1-1 to SLS2-4, respectively, are uplifted into a fault-propagation fold controlled by a steep (~60°) reverse fault on the western edge of the basin (CMP ~14000). This reverse fault extends almost to the seafloor but is locally buried by a very thin (< 100 m) blanket of sediments. Nevertheless, two hinges of the fault-propagation and adjacent (CMP ~13100) folds crop out along the seafloor (Figure 5c) and abundant local seismicity, although the depth uncertainty of the focal mechanisms is large, suggests that uplift may be still active here (Figure 2). The shallowest tectonostratigraphic package spans from SLS2-4 to the seafloor and exhibits strong lateral thickness variations and is mostly flat lying. This package thins and onlaps uplifted structures on the western edge of the basin near Puysegur Ridge and is locally thin at the crest of the open fold beneath Solander Channel, while gradually increasing in thickness away

from the hinge into the adjacent flanks. East of CMP ~8500, the upper boundary is an erosional surface as the seafloor truncates angularly across the flat stratigraphy.

4.2 SISIE-2 – Northern Regional Dip Line

SISIE-2 comprises the second regional margin-perpendicular profile and runs for a total of 281 km long at ~47.5°S, of which ~180 km of MCS, OBS, and bathymetry data are shown in Figure 6. SISIE-2 is oriented obliquely (~45°) to the oceanic abyssal hill fabric, characterized by rough volcanic basement highs outcropping at the seafloor and sparse, thin pockets of sediment infilling basement lows. Our seismic velocity model reveals a 5-6 km-thick incoming oceanic crust with velocities similar to those imaged on SISIE-1, with the exception of a slight reduction in upper mantle V_p (~7.4 km/s) on the SISIE-2 profile. The incoming oceanic plate remains flat at ~4.5 km depth until seafloor-breaching normal faults are first encountered approximately 10 km from the trench at CMP ~20250. From CMP ~20250-22000, three major normal faults offset the basement with throws of ~800, 900, and 1300 m, respectively, in a staircase-like fashion. Across this faulted zone, the sediment cover promptly increases in thickness from a few hundred meters to ~1.5 km directly beneath the trench axis. Beneath this faulted zone, we observe a reduction in upper mantle seismic velocities to ~7.0 km/s.

East of the trench, we image a high-amplitude reverse-polarity reflection that overlies ~1.5 km of sediments, which in turn overlie the Australian oceanic basement (Figure 6a). This reverse-polarity reflection has an average dip of ~10° and is semi-discontinuous, yet the overall sequence of sediments beneath this reflection is well imaged for approximately 20 km laterally beneath the overriding Pacific Plate. Above this reflection, we find highly folded and faulted sediments with offsets indicating thrust relationships, and V_p between 2-4 km/s.

We interpret this reflection to be the décollement separating the lower and upper plates and the overlying strata as accreted sediments (Figure 6a). The rapid west to east increase in trench fill accommodated by normal faulting suggests that most of the subducting and accreting sediments are not likely sourced from the Australian Plate but rather from sediment sources to the north.

The accreted assemblage continues to the east for approximately 30 km. At CMP ~24000, a major reverse fault overthrusts a package of east-dipping strata with minor internal deformation. As the package thickens and seafloor shallows, a reverse-polarity Bottom Simulating Reflection (BSR) is imaged from CMP ~25000-26500. The base of the sedimentary pile is unclear, but in some areas a bright reflection marks the base of continuous sedimentary reflections (CMP ~25000, ~7.5 km depth; CMP ~26000, ~4.6 km depth) and is accompanied by a slight increase in seismic velocities ~4 to ~5 km/s (Figure 6a, 6e).

At CMP 26250, a thrust fault juxtaposes opaque basement laterally with folded strata, which is unconformably overlain by a thin drape of mostly undisturbed sediments. From here to the axial valley of the Snares Zone, the underlying basement appears opaque and has similar seismic velocities (~4-6 km/s) to the western flank of Puysegur Ridge imaged on SISIE-1. Across the Snares Zone, we observe several basement offsets that suggest steeply dipping faults. In a pocket of sediment at the central depression of the Snares Zone, we image a near vertical fault juxtaposing flat-lying strata to the west with folded strata to the east, suggesting a strike-slip relationship. We observe a relatively sharp increase in crustal seismic velocities across the axial valley of the Snares Zone, consistent with observations from SISIE-1. Focal mechanisms indicate primarily strike-slip motion on near vertical faults throughout the Snares Zone (Figure 2). Our tomographic image is not well resolved beneath the axial valley of the Snares Zone (Figure 4), but slightly to the east, wide-angle Moho reflections suggest the crust may be up to 14 km thick. Eastern Puysegur Ridge appears to be mostly comprised of crystalline rocks cropping out along

the seafloor, with V_p increasing from ~ 4.5 km/s to ~ 7 km/s at 14 km depth near the crust-mantle boundary.

Images of the Solander Basin on SISIE-2 uncover a more variable basin architecture than southern Solander Basin on SISIE-1. The basin here is ~ 55 km wide and exhibits strong asymmetry in sedimentary thickness, depositional patterns, and underlying crustal structure. First-order basement geometry exhibits large topographic relief offset by a series of east-dipping, low-angle ($\sim 30^\circ$) normal faults. Highly asymmetric, tilted crustal blocks are often separated by more than 2 km of vertical relief along the bounding faults, which curve at depth in a listric fashion. Deepening of the basement to the east results in crustal thinning to a minimum of 6 km near CMP 40500. Along the western crustal block (central CMP ~ 35000), the basement reflection is mostly coherent, high-amplitude, and marks a sharp impedance contrast between overlying sediments and crustal rocks. Between CMP ~ 35500 -40000, we detect a thin zone of chaotic reflectivity above the basement, with several pointed structures near CMP ~ 38000 , similar to the interpreted volcanic layer found on SISIE-1. Intracrustal reflectivity is less abundant than on SISIE-1, and crustal V_p increases from ~ 5 km/s near the top of basement to ~ 7 km/s in the lower crust, with no regions of anomalously high V_p observed on this profile.

Sedimentary thickness varies across the basin and is highly dependent on crustal geometry, generally increasing from west to east up to a maximum thickness of 6 km above the thinnest crust near the eastern edge of the basin (CMP ~ 40000). Deep sedimentary reflectors within easternmost Solander Basin are abruptly truncated laterally at CMP ~ 41000 . East of this truncation, a scrambled and structurally complex zone underlies flat-lying sediments between CMP ~ 41000 -42500, which may be obscuring clear imaging below. The top of basement is possibly imaged at 6.5 km depth near CMP ~ 41500 and the seismic velocities of the overlying material have $V_p < 5$ km/s.

We interpret this complicated zone as highly deformed sediments. Although the area is poorly imaged, the structural position of the basement and deformed zone can be explained by a thrust fault near CMP ~ 41000 , which may have uplifted the basement and caused the inferred folding.

We establish four distinct tectonostratigraphic intervals within Solander Basin on SISIE-2. The deepest interval (top of volcanic layer to SLS1-1) has strong divergent fill geometries in two main wedges between adjacent crustal blocks, indicating deposition coeval with tectonic extension. In the deepest part of the basin, this wedge has high velocities ($V_p > 5$ km/s) and transitions from zero thickness onlapping the volcanic layer to ~ 2.3 km thick over a lateral distance of just ~ 12 km (Figure 6b). Between CMP ~ 36500 -38500, this interval is not clearly identified, possibly due to non-deposition because of local relief, or was eroded and/or entirely overprinted by volcanism.

The second tectonostratigraphic sequence spans SLS1-1 to SLS2-1 and consists of mostly subparallel reflections that onlap volcanic features atop a crustal block between CMP ~ 36500 -38500. The upper boundary is marked by a high amplitude reflection across the basin and can be traced eastward at the top of the highly deformed zone.

Between SLS2-1 to SLS2-3, we define a third tectonostratigraphic package because the interval strongly thins towards and caps the uplifted zone along eastern Solander Basin, indicating deposition syn-kinematic with compression and shortening. This interval is also locally folded and faulted above volcanic highs (CMP ~ 36500 -38500) and folded onto the westernmost buried crustal block (CMP ~ 35300), although it is unclear if these features are depositional, due to differential compaction, or truly tectonically driven in nature.

The shallowest tectonostratigraphic package extends from SLS2-3 to the seafloor and contains mostly undeformed sediments. This package has mostly uniform thickness in the middle of the basin but thins and onlaps against Puysegur Ridge in the west, and onto the Campbell Plateau in the east.

4.3 SISIE-3 – South-North Variations in Solander Basin

SISIE-3 is oriented subparallel to the margin and transects Solander Basin, providing along strike images of basin architecture and a regional seismic tie between SISIE-1 and SISIE-2 (Figure 7). The uppermost crust on this profile is rough and consists of discontinuous, bright, and high-amplitude serrated reflections. This rough upper crust is consistent with the interpreted volcanic domains imaged on SISIE-1 and SISIE-2. The bounding upper reflector is very rugged with high relief in the south, but gradually becomes smoother and sharper as it shallows to the north forming a topographic high. We do not observe a clear basement reflection throughout most of the profile.

Intracrustal reflectivity is widespread on SISIE-3, especially along the southern half of the profile. Between CMP 20000 and 28000, we observe a 50-km-wide and ~6 km-thick region of bright reflections beneath the top of the volcanic layer (Figure 7). These reflections are characterized by high amplitudes, low frequency, and moderate continuity and they exhibit transgressive, stepwise transgressive, subhorizontal, and curved geometries.

We interpret this zone of high intracrustal reflectivity as an organized complex of magmatic intrusions. Similar structures have been imaged and drilled at volcanic rifted margins, typically within sedimentary host rocks (Eide et al., 2018; Schofield et al., 2017; Thomson & Hutton, 2004), but also deeper within the crust (e.g. White et al., 2008). Although we do not have OBS data coincident with SISIE-3 to help constrain seismic velocities in the crust, a move-out analysis with our long-offset streamer suggests reflections from this zone are flattened best with interval velocities of $V_p > 7$ km/s, indicating a largely mafic composition. Reflection strength (Figure 7b) and instantaneous phase seismic attributes (Figure 7a) at CMP ~20000-24000 show that magmatic intrusions are mostly south-dipping at ~25°. These features appear to be truncated by shallower north-dipping (~15°) intrusions and a large subparallel curved sill at ~7 km depth, spanning a lateral distance of ~25 km. Above this large curved sill, numerous volcanic cones suggest melts from magma reservoirs may have fed vent-style eruptions. In contrast, at CMP 20000-22000, dikes/sills appear to merge with flat-lying, semi-continuous and bright reflections, which are more consistent with extrusive fissure eruptions and large volcanic flows (Figure 7a, 7b).

Along the seismic profile SISIE-3, numerous deep faults can be distinguished from other intracrustal reflectivity by their continuity and clear connection to offsets in the volcanic layer and stratigraphy. Crustal faults are more abundant on the northern half of the profile, while only a few faults are identified on the southern half (Figure 7). Structural relationships indicate that faults display mostly normal offsets and become listric at depth with low average apparent dips of ~40°. Several of the synthetic/antithetic fault-pairs appear to cross-cut each other, evidenced by slight offsets in fault plane reflections (Figure 7b), suggesting a complicated poly-phase deformation history. Individual faults also show evidence of a polyphase history; for example, we detect a significant fault starting from the seafloor at CMP ~18000 which offsets the entire basin stratigraphy at ~60° and curves to ~35° at ~20 km depth, potentially rupturing through the entire crust. This fault appears to have reverse offsets across the top of the volcanic layer and horizon SLS1-1, little to no offset across SLS2-1, and normal offset relationships from SLS2-2 to the seafloor, indicating it may have been earlier active as a reverse fault and was later re-activated and currently active as a normal fault (Figure 7). We find a similar but flipped sequence on a fault in the south at CMP ~29500, which offsets the top of the volcanic layer in a normal sense through

SLS2-2, but shows little to no offset across SLS2-3 and reverse offsets from SLS2-4 to the seafloor. These observations suggest it was initially a normal fault and was later re-activated and is currently an active reverse fault (Figure 7).

4.4 SISIE-6bc – Northern Solander Basin

SISIE-6bc is oriented southwest-northeast and extends from the western edge of Solander Basin near the Snares Zone onto the continental shelf of the South Island. Our seismic image for profile SISIE-6bc (Figure 8) is a composite of two separate PSDM lines, originally called MCS17B and MCS17C. The SISIE-6bc profile crosses obliquely over Tauru High, an uplifted structure caused by intense reverse faulting and folding (Melhuish et al., 1999; Sutherland & Melhuish, 2000; Patel et al., 2020), which we refer to as the Tauru Fault Zone (TFZ). The TFZ consists of four deep-seated crustal faults which can be traced to the Moho (Figure 8b).

South of the TFZ, the basement is well imaged and overlain by a thin rough transitional upper crust. The basement here is cut by shallow ($\sim 20^\circ$) normal faults with little throw except for a large normal fault at CMP ~ 7500 which offsets the basement and volcanic layer by greater than 1.5 km. The basement is not well imaged beneath the TFZ on the northern part of SISIE-6b, because severe weather forced us to tow a smaller airgun source at 18 m depth and caused streamer feathering. From CMP ~ 3500 to the northern end of SISIE-6c, the basement is well imaged and capped by a thin layer of semi-discontinuous high-amplitude reflections (Figure 8b).

Some intra-crustal reflectivity is observed throughout the profile, mostly in the mid-lower crust along SISIE-6c, although we cannot confidently rule out that some of these bright events may be residual multiple energy or out-of-plane reflections. Moho reflections are clear throughout most of the line around 16-18 km depth; thus, crustal thickness is just 7 km adjacent to the TFZ (CMP ~ 10000) and increases to greater than 14 km in the north along the continental shelf.

The multifaceted tectonic and sedimentary history of the basin has resulted in a complicated stratigraphic architecture. A seismic well tie is relatively straightforward at the Parara-1 borehole, resulting in a 1D age-depth model derived from biostratigraphic analyses of recovered rocks (Hunt International Petroleum Company, 1976) that can be tied to older industry seismic lines (e.g., Sutherland et al., 2006) and to the SISIE dataset (Patel et al., 2020). Extending this stratigraphic framework throughout the entire Solander Basin is challenged due to sparse seismic coverage, and unfortunately crucial line crossings are above basement highs (SISIE-6b/SISIE-2, SISIE-2/SISIE-3, see Figure 6) where most of the deeper stratigraphic record has either been eroded or not deposited. This difficulty is especially severe for the deepest stratigraphic intervals, for example on SISIE-6c, which are missing just south of the Parara-1 borehole where Middle Miocene sediments unconformably overlie basement (Patel et al., 2020). Therefore, a unique correlation cannot be established throughout the basin.

Patel et al. (2020) divided stratigraphic intervals based on internal seismic-reflection character, stratal stacking patterns, and sequence boundary relationships with initial post-stack time migrated images. The pre-stack depth migrated sections presented in this paper were generated with more advanced processing techniques which have significantly improved imaging of the deeper strata, basement, and crustal structure across the TFZ. We re-visit the correlation of stratigraphic units across the TFZ in light of our new depth-migrated seismic images. Correlations are based on structural characteristics of stratigraphic intervals, including reflection geometries, thickness variations, and deformation associated with folding and faulting.

At the fold crest atop Tauru High (CMP ~ 11600), a ~ 1.5 km thick package of conformable sediments is asymmetrically folded and emergent at the seafloor. The base of this package is marked by a high-amplitude reflection at ~ 3 km depth, which can easily be traced from the axial

plane throughout the entire forelimb and eastward along the backlimb. This reflection could be interpreted as the basement since it is a high amplitude return and deeper reflectivity has less continuity. On the other hand, beneath this reflection, our new PSDM reveals a deeper ~1.5 km thick package with the lower boundary marked by a bright, semi-discontinuous reflection near ~4.5 km depth. Even though it is less coherent, the internal reflectivity of this deeper package has moderate amplitude and structural continuity with reflectors following an asymmetric fold pattern, similar but more tightly folded than the overlying strata.

Based on the internal structure and continuity of the bounding reflectors, we interpret this zone as consisting of highly deformed sediments that overlie the basement. This deepest package is thinnest at the axial plane and thickens both into the fore and backlimbs, indicating it was deposited syn-kinematically with extension at the TFZ. Thus, we re-interpret the upper boundary of unit SLN1-1 to represent the top of the syn-extensional stratigraphic package at the TFZ (CMP ~10000 on SISIE-6b to CMP ~3750 on SISIE-6c), consistent with observations at the Parara-1 borehole (Patel et al., 2020).

South of the TFZ, the sedimentary fill reaches ~6 km, which is the thickest succession observed throughout the entire basin. The deepest strata onlap basement highs and exhibit divergent and prograde fill reflection configurations, with growth wedges at CMP ~7500 and towards the TFZ near CMP ~10000, consistent with a syn-extensional origin. The upper boundary of this package is marked by a subtle moderate amplitude reflection at ~4.5 km depth, where a transition occurs to subparallel and flat reflections in the overlying stratigraphy. Therefore, we re-interpret the top of unit SLS1-1 south of the TFZ as the top boundary of the syn-extensional stratigraphy (Figure 8a, 8b). No additional updates were made to the interpretation of unit boundaries, as the shallow stratigraphy in our PSDM images was not significantly different than the shipboard time-migrated images. Patel et al. (2020) interpreted the SLS1-1 unit as representing syn-rift sediments followed by a hiatus and correlated this unit with both SLN1-1 and SLN2-1 across the TFZ. Alternatively, our images suggest the southern unit is entirely syn-rift and thus we prefer to correlate SLS1-1 with our revised SLN1-1 across the TFZ. This correlation suggests that the TFZ accommodated minor and distributed Eocene-Oligocene extension (Figure 8, Figure S2), in contrast to the major and focused extension inferred in Patel et al. (2020).

We define a second tectonostratigraphic interval from SLS/SLN1-1 to SLS2-1/SLN2-1. This interval has mostly constant thickness across the profile and continuous and conformable reflections. Along the backlimb of the TFZ the interval is slightly thicker (~1.5 km) and strata downlap the SLN1-1 reflector (CMP ~1000, SISIE-6c). Strata are horizontal and undeformed adjacent to the structurally lowest thrust of the TFZ, suggesting it predates reverse activity on the TFZ. Therefore, we correlate SLS2-1 with SLN2-1 and interpret this tectonostratigraphic interval as post-rift sediments, with minor thickness variations reflecting the infilling of topography created during extension and/or post-extension subsidence.

The third tectonostratigraphic package on SISIE-6bc extends from SLS/SLN2-1 to SLS2-3/SLN3-1. We distinguish this stratigraphic interval based on strong thickness and tilting relationships across the TFZ. Sediments of this interval crop out at the seafloor along the hinge of the Tauru High. Here, this interval is only a few hundred meters thick, but rapidly thickens to the northeast in a divergent pattern along the backlimb of the TFZ. South of the TFZ, strata quickly become tilted and pinch out against uplifted deeper tectonostratigraphic packages of the thrust front (CMP ~10000). Near the fold crest this interval is absent, suggesting that the thrust sheets of the TFZ were emergent and pre-kinematic strata were likely eroded at this time. These structural relationships indicate that deposition of this interval was syn-kinematic with reverse faulting on

the TFZ. Based on respective similarities in the thickness variations and onlap patterns across the TFZ, we correlate SLS2-2 with SLN2-2 and SLS2-3 with SLN3-1 (Figure S2). Imaged geometries are in excellent agreement with the expected architecture of a thrust-system with high sedimentation rates during tectonic activity (e.g., Butler, 2019). The continuous presence of syn-thrust strata throughout the basin is consistent with a significant increase in sediment supply during deposition of these units (Patel et al., 2020; Sutherland et al., 2006). Thicker syn-thrust strata along the backlimb of the TFZ suggests that the emergent thrust sheets became a structural barrier and trapped sediments transported from the north. Our interpretation of the structural architecture of the TFZ indicates that the fault zone was inherited from earlier extension, however it was more active and accumulated greater offsets during its inversion history.

Lastly, from SLS2-3/SLN3-1 to the seafloor, strata are generally internally conformable and subhorizontal. Strata thin towards the TFZ and are missing from the crest of the Tauru High, indicating that the highest thrust sheet remains emergent at the present-day seafloor. We do not image any clear evidence indicating obvious tectonic activity during deposition of this interval. Therefore, we interpret this shallowest tectonostratigraphic package as post-thrust deposition during tectonic quiescence.

4.5 SISIE-8 – Continental Shelf near South Island

SISIE-8 is oriented west-east and runs along the continental shelf proximal to the South Island and extends westward onto Puysegur Bank (Figure 9). This region of the margin has been surveyed by industry seismic lines and the stratigraphy has been tied to petroleum boreholes, core, and dredge data (e.g., Sutherland et al., 2006). From west to east, SISIE-8 crosses over Puysegur Bank and the Balleny and Waitutu sub-basins, which are separated by the Eastern Balleny Fault and the Hauroko Fault (Turnbull & Uruski, 1993). Stratigraphic horizons from the Parara-1 well (Patel et al., 2020) were successfully correlated from SISIE-6 into the Waitutu sub-basin, but were not correlated into the Balleny sub-basin due to complex structural variations across the Hauroko Fault.

At the eastern edge of the profile, we image the reverse Solander Fault (CMP ~2750) and associated folded sediments forming the Solander Anticline (Figure 9a). Throw across the fault gradually decreases at shallower depths leading us to interpret this structure as a fault-propagation fold, and the crest of the fold is truncated and eroded at the seafloor, indicating that this structure is likely still active. Originating from the footwall ramp of the Solander Fault (~2.5 km depth), we find a pattern of short, discontinuous and bright reflectivity that obliquely crosses dipping stratigraphy and can be tracked to the seafloor near CMP ~4500. A similar vertical column of scattered reflectivity rises to the seafloor at the same location, close to the Solander Island volcano.

The Waitutu sub-basin begins near CMP ~4000 marked by deepening of the basement to ~5 km depth and a large increase in the sedimentary fill to ~4.5 km. Strata throughout the sub-basin are consistently dipping to the east, with deeper beds tilted slightly steeper ~7° compared to shallower beds at ~4°, which are truncated at the seafloor. The deeper stratigraphy is not as well imaged, but growth wedge geometries indicate there may be greater than 2 km of syn-extensional sedimentary deposits here. Farther to the west, at the crossing of Hauroko Fault (CMP ~7000), we observe a ~1 km-wide seismic blank zone with no coherent reflections. Just west of the blank zone, basement appears at ~1 km depth and the stratigraphy is gently dipping to the west. The Balleny Basin is characterized by an erratic blocky crustal morphology cut by many faults and folded/faulted stratigraphy, implying a complicated tectonic history with intense deformation. At the Eastern Balleny Fault (CMP ~16500), we observe another seismic blank zone which juxtaposes basement at ~4 km depth and east-dipping strata in the Balleny Basin with a shallow basement and

a thin (<1 km) drape of sediment atop Puysegur Bank. The basement beneath Puysegur Bank is highly irregular, overlain by segmented pockets of deformed sediments. At the western edge of the line, basement deepens to ~3 km and a BSR reflection is observed from CMP ~19500-20000 in the overlying sedimentary column.

5. Regional Interpretation of Key Tectonic Structures

The integration of new high-quality MCS data together with tomographic images from wide-angle seismic data allow us to interpret regional subsurface structures throughout the entire Puysegur Margin. We reconcile our observations with previous findings and broader Cenozoic reconstructions of the Australian-Pacific plate boundary.

5.1 Continental Rifting in the Solander Basin

The data presented in this study provide evidence that the Solander Basin contains extended crust to at least 49.5°S. Furthermore, we infer that the Solander Basin crust is continental in nature based on the following lines of evidence: (1) the basement reflection in most places is coherent, continuous, and smooth; (2) normal faults slice the crust into planar fault-bounded blocks; (3) normal faults are listric in nature, invoking tilting and rotation of the crustal blocks; (4) wedge-shaped geometries of the deepest sediments are consistent with expected syn-extensional relationships. Furthermore, recovered samples from the Parara-1 borehole were largely terrestrial sandstones with coal deposits; (5) crustal thickness ranges between ~6-15 km; (6) seismic velocity structure of the crust is consistent with extended and intruded continental crust found at other rifted margins; and (7) seismic velocities resolved in the upper mantle are typical for peridotite (~8 km/s), in contrast to reduced velocities found in the upper mantle of the slow-spread oceanic lithosphere along the incoming Australian Plate.

Without the insight from deep penetrating and regional geophysical data coverage, previous studies proposed that the Solander Basin contains Eocene-Miocene age oceanic lithosphere (Lamarche et al., 1997; Lebrun et al., 2003; Sutherland et al., 2006), assuming a northward continuation of the MSC (e.g., Keller, 2004). The prevailing hypothesis suggested a sharp Continent-Ocean Transition (COT) along the entire western edge of Campbell Plateau which curved west and cut across the Solander Basin just south of the Tauru Fault (~48°S). This COT separated the oceanic domain created by seafloor spreading (commonly referred to as “Solander Trough” in literature, e.g., Sutherland & Melhuish, 2000) from the extended continental domain in northern Solander Basin and other subbasins along the shelf of southern New Zealand. Instead, we find no evidence for normal oceanic lithosphere and propose that the continental basement of the Solander Basin formed by Eocene-Oligocene stretching between the Campbell and Challenger plateaus. In this scenario, complete continental breakup was never achieved this far north and hence did not proceed to seafloor spreading in the Solander Basin.

Continental rifting between the Campbell and Challenger plateaus was accompanied by a north-south progression in the amount of extension. For example, the width of the Solander Basin is ~55 km along SISIE-2, however it becomes more than twice as wide (>120 km) in the south along SISIE-1. Crustal structure indicates fewer extensional faults with larger throw create greater basement relief in the north, compared to more closely spaced faults and lower average basement relief imaged in the south. Moreover, the faulting geometry is highly asymmetric in the north with dominantly east-dipping faults, whereas a mix of east- and west-dipping faults form horst-graben structures in the south on SISIE-1. The overall rift architecture argues that continental rifting was more advanced in the south, and perhaps opened in a “V-shape” geometry.

To quantify the amount of extension that occurred during Eocene-Oligocene rifting, we first calculate 1-D crustal thickness values across the SISIE-1 and SISIE-2 profiles. Two crustal

thickness values are considered, using the base of crust (Moho) depth constrained solely by OBS data and the top of crust (basement) from both OBS and MCS images. We compute 1D isotropic crustal stretching factors (β) with the present-day crustal thickness values, with the simplified assumption that extension is uniform throughout the crust at a given horizontal location along the profiles (e.g., Davis & Kuszniir, 2002). Gravity data suggest that the crust is uniformly ~20-24 km thick across the Campbell and Challenger plateaus (Grobys et al., 2008; Hightower et al., 2019); therefore we choose a constant pre-rift crustal thickness of 21 km in our β calculation. Lastly, the total amount of extension is calculated by integrating β along the width of the margin for each profile, respectively. Our results indicate that approximately 45 km of total extension occurred along SISIE-2 and ~64-69 km of extension along SISIE-1, supporting other evidence that continental rifting was more pronounced in the south (Figure S1). These values represent absolute minimum estimates of tectonic extension for several reasons. Firstly, because the MCS data along SISIE-1 do not extend onto the Campbell Plateau due to equipment malfunction during data collection; therefore, we cannot account for some crustal thinning at the easternmost edge of the basin. Additionally, we observe $\beta \sim 1.7$ at eastern Puysegur Ridge on SISIE-1, which suggests that a small portion of thinned crust may have existed to the west of the Puysegur Fault. Secondly, because our seismic images indicate a contribution of magmatic additions, which have increased the thickness of the crust. To account for the second point, we make a very simplified assumption that lower crust with $V_p > 7.1$ km/s represents mafic additions (Figure S1). Removing the magmatic component and recalculating the total extension yields ~74 km for SISIE-1 (15.6% increase) and ~47 km for SISIE-2 (4.4% increase). These findings are lower than the median values predicted by past plate motions (~90±105 km in the north and ~140±80 km in the south, Keller, 2004) but are within the large uncertainties, and in good agreement with estimates from seismic studies of northern Solander Basin (~50-100 km, Sutherland and Melhuish, 2000). Overall, our observations of greater extension to the south support a wedge-shaped opening in agreement with plate reconstruction models, since the AUS-PAC rotation pole was located proximal to the South Island (e.g., Cande & Stock, 2004).

We investigate whether the magmatic intrusions and extrusive volcanism throughout Solander Basin may be linked with the Eocene-Oligocene episode of continental rifting or other tectonic processes. It is well known that lithospheric extension in continental rifts can involve mantle upwelling and decompression melting, leading to magmatic intrusions and volcanic eruptions (e.g., Bown & White, 1995). Conversely, Late Cretaceous to Miocene intraplate volcanism was widespread across Zealandia (Mortimer et al., 2018; Timm et al., 2010), therefore overlapping with the period of continental rifting and may have contributed to the features imaged in our study. High velocity lower crust ($V_p > 7.1$ km/s), indicative of mafic intrusions, is abundant throughout SISIE-1, but limited/absent on SISIE-2, suggesting that more pervasive mantle melting occurred in the south. This suggestion agrees with spatial variations of bright intracrustal reflectivity in the MCS data, which are more abundant in the south (for example the sill complexes on SISIE-1 and SISIE-3), further suggesting that crustal extension led to magmatism. Imaged crustal faults apparently terminate into sill complexes where fault-plane reflectivity shifts to higher amplitudes and lower frequencies (Figure 5b). This observation suggests that fault zones may have provided pathways for migrating melts, thus tectonic deformation and magmatic activity were likely coeval. In the upper crust, volcanic features, such as cones and lava flows, primarily only alter/overlap with syn-rift strata (Figure 5b, 7b), indicating an Eocene-Oligocene age for these features. If the volcanic structures within Solander Basin were largely related to regional Cenozoic Zealandia volcanism, we would expect to image evidence of volcanic activity altering the

shallower basin stratigraphy (i.e. not only directly overlaying the basement). Only one clear example of this potential alteration exists on the western edge of the basin on SISIE-1 (CMP ~14600) where the stratigraphic column is disturbed and several bumps crop out along the seafloor (Figure 5c, 5d). We therefore conclude that the dominant age of magmatic emplacement within Solander Basin is Eocene-Oligocene and is tectonically related to decompression melting beneath the developing continental rift zone between the Campbell and Challenger plateaus.

5.2 Strike-slip Deformation and Transition across Puysegur Ridge

We find evidence in our seismic reflection images and wide-angle tomography models for a major lateral change in subsurface velocities and crustal structure west of Puysegur Ridge. At the axial valley of Puysegur Ridge on SISIE-1, we detect a sharp decrease in crustal Vp from east to west (Figure 5e). Because the resolution of our tomographic image beneath Puysegur Ridge is sufficient (Figure 3), we consider this relatively abrupt velocity contrast a robust feature with geologic significance. We do not image a concurrent fault trace in the reflection image, although imaging is challenged here by scattering of seismic signals and overwhelming multiple energy, caused by rugged seafloor topography and a high acoustic impedance contrast at the seafloor due to basement cropping out along the ridge. Likewise, on SISIE-2, we detect a decrease in crustal Vp from east to west across the axial valley of the Snares Zone. The resolution of our tomography model in the lower crust here is poor, although the velocity contrast is still evident in the upper-middle crust where velocities are better resolved (Figure 3). In the SISIE-2 MCS image, we detect numerous basement offsets and associated folding in the thin sedimentary cover across the Snares Zone, including an obvious strike-slip fault within the axial valley (CMP ~30000). Although we do not have wide-angle seismic constraints farther north, the Eastern Balleny Fault on SISIE-8 clearly marks a significant transition in crustal structure, separating the blocky rifted continental crust domain on the east from uplifted and structureless basement on the west. It is therefore reasonable to assume that this tectonic boundary is potentially continuous and extends from the axial valley of Puysegur Ridge in the south, northward through the Snares Zone, and along the eastern flank of Puysegur Bank. We interpret this boundary, the Puysegur Fault zone, as the seaward limit of the rifted continental crust domain, and suggest that the lithosphere to the west is primarily translated to the north in a similar direction as the Australian Plate.

The distribution of strike-slip deformation varies strongly along the Puysegur Fault zone. At the southern margin, earthquake focal mechanisms, the lack of imaged faults, and morphology of the ridge suggest that dextral strike-slip and transpressional deformation is localized to the axial valley of Puysegur Ridge (Figure 2). In contrast, we image many near-vertical faults across the Snares Zone on SISIE-2, indicating that deformation is likely accommodated across a broader shear zone. Seismicity is widespread throughout the Snares Zone (Figure 2) and bathymetry data clearly show northeast directed and distributed shear characterized by fault-bounded, en échelon ridges forming Puysegur Ridge (Lamarche and Lebrun, 2000). We find no evidence for significant active strike-slip deformation east of Puysegur Ridge and south of the Tauru Fault. The lack of major strike-slip structures throughout the Solander Basin suggests that strike-slip deformation has primarily occurred near Puysegur Ridge since the late Oligocene. North of the Snares Zone, the number of near-vertical structures increases again over a broader expanse resulting in a spatial defocusing of strain. Visible scarps on the seafloor atop Puysegur Bank indicate recent strike-slip on multiple fault strands (Melhuish et al., 1999; Sutherland & Melhuish, 2000). These faults strike N-S, whereas the Hauroko, Solander, and Parara faults farther to the east trend NE-SW. Our seismic images support at least two major, active zones of dextral strike-slip and oblique reverse motion along the Hauroko and Eastern Balleny faults. The Hauroko Fault forms the southern

extension of the Moonlight Fault System, which extends onshore and correlates with a complex zone of dextral strike-slip and high-angle reverse motion (Norris et al., 1978). The similarity in the strike of the Puysegur and Hauroko faults suggests that they may have been previously connected as part of the larger strike-slip plate boundary during the Oligocene (Lamarche & Lebrun, 2000; Lebrun et al., 2003); however, seismic reflection data show undeformed Middle Miocene and younger strata across the southern Hauroko Fault (Sutherland et al., 2006), indicating a lack of structural continuity since this time. The broad zone of strike-slip faults dissecting the continental shelf of the South Island suggests that a primary change from focused to distributed strike-slip deformation starts near the Snares Zone and continues throughout the northern Puysegur margin.

5.3 Reactivation of Rift Structures during Subduction Initiation

We have found subtle evidence for structures related to compression in the overriding plate throughout the entire length of the offshore Puysegur margin. According to geodynamic models, the arrival of compressional stress is associated with the initial stages of subduction as convergence is resisted (Toth & Gurnis, 1998). Therefore, the location and timing of uplift in the Pacific Plate provide constraints on subduction initiation at the Puysegur Trench. Most of the compressional structures imaged in our study show a clear history of previous extension and/or strike-slip, indicating that inherited tectonic structures were important in the reorganization and evolution of the AUS-PAC plate boundary. Using an updated chronostratigraphic framework originally from Patel et al. (2020), we are able to determine the approximate timing of these tectonic features.

The earliest (~16 Ma) evidence of reactivation is observed on SISIE-6bc and consists of widespread uplift at the TFZ. Inversion of the TFZ occurred simultaneously with abundant sediment delivery into the basin, trapping sediments adjacent to thrust sheets and along the main backlimb depression. Compression across the margin also induced reverse faulting and associated folding of the basement and overlying syn- and post-rift deposits at the eastern edge of central Solander Basin on SISIE-2. We do not find any evidence for compressional structures in southern Solander Basin at this time. We interpret this episode of broad and rapid uplift as a dynamic response to large compressional stresses in the upper plate resulting from early underthrusting near Puysegur Bank.

Tectonic activity in the upper plate across the northern and central margin slowly waned starting at ~14 Ma. Uplift of the Campbell Plateau diminished and was largely inactive around ~11.5 Ma, however inversion at the TFZ continued until ~8 Ma, and minor inversion on the Parara Fault slightly to the north commenced at this time. We believe this signal reflects the gradual spreading and progression of the nascent subduction, which caused expanding compressional stresses in the upper plate.

An evolving wave of shortening spread out along the margin between ~8-5 Ma. In the early Pliocene, oblique reverse slip became active on the Parara, Solander, and Hauroko faults along the continental shelf and minor transpressional activity ramped up in southern Solander Basin. In contrast, passive onlapping of sediments in the central/northern Solander Basin argue for the cessation of compressional stresses in this section of the margin. We suggest that these spatial stress-strain relationships record the along-strike propagation of the subduction interface to both the north and south, and continued maturation and relaxation surrounding the site of initial underthrusting.

Two westward verging reverse faults along the western edge and a broad open fold in the center of Solander Basin at the southern Puysegur margin became active around ~5 Ma, deforming syn- and post-rift strata. We interpret this tectonic signal as marking the early stages of subduction at the southern margin. Visible disturbance at the seafloor indicates that large compressional

stresses are still present here. Furthermore, the presence of a significant accretionary prism at the northern Puysegur Trench (Figure 6) and very minor accreted sediments at southern Puysegur Trench (Figure 5) likely reflect increased accommodation space, sediment supply and a longer history of subduction to the north, indicating a southward propagation of the trench over time.

6. Discussion

6.1 Revised Pacific Plate Continent-Ocean Transition (COT)

Previous tectonic interpretations claimed that the southern Solander Basin is floored by Eocene-early Miocene aged oceanic crust that was created by the Macquarie Spreading Center (MSC), which propagated northward and created new oceanic crust following rifting (summarized by Lebrun et al., 2003). This model implies rapid breakup of the Challenger and Campbell plateaus and the existence of conjugate COT pairs. Sutherland and Melhuish (2000) suggested that the MSC propagated north to at least $\sim 48^{\circ}\text{S}$, just south of the Tauru Fault Zone. However, the new evidence strongly argues that the Solander Basin is a failed continental rift at least north of $\sim 49.5^{\circ}\text{S}$. Furthermore, we find no evidence that true seafloor spreading was active in the Solander Basin at any time. We conclude that the Campbell Plateau rifted margin is much wider and longer than previously thought and that the northern propagation limit of the MSC must be south of $\sim 49.5^{\circ}\text{S}$.

The latitude marking the transition from seafloor spreading along the MSC to continental rifting between the Campbell and Challenger plateaus is a key constraint for regional plate tectonic reconstructions. While the SISIE dataset only extends to $\sim 49.5^{\circ}\text{S}$, we revisit previous observations and global datasets to define a new boundary between the oceanic and continental domains (COT) of the Pacific Plate, and revising our preliminary SISIE interpretations which placed the transition south of 49° (Gurnis et al., 2019). Tectonic reconstructions along the MRC are largely based on magnetic anomaly and fracture zone correlations (Cande & Stock, 2004; Keller, 2004; Lebrun et al., 2003; Massell et al., 2000). No clear fracture zones have been identified in the Solander Basin. The northernmost potential fracture zone on the Pacific plate (Te Awa, Massell et al., 2000), albeit controversial, extends from the McDougall-Puysegur trench transition at $\sim 50^{\circ}\text{S}$ and curves to the edge of the Campbell Plateau at 51.5°S . The northernmost undisputed fracture zone for which a conjugate visible on the Australian plate exists is FZ9 (Hayes et al., 2009; Keller, 2004), which extends from the MRC at $\sim 51.5^{\circ}\text{S}$ and curves counterclockwise to $\sim 55.5^{\circ}\text{S}$, where it terminates against north-south Emerald Basin fracture zones. Concurrently, the northern extent of clear magnetic anomalies is just north of FZ9 up to $\sim 54^{\circ}\text{S}$, where the ocean crust ranges from ~ 40 - 30 Ma (Keller, 2004). Bathymetry and free-air gravity grids show several significant bathymetric highs that have a blocky appearance, extending horizontally between the MRC and Campbell Plateau at $\sim 51^{\circ}\text{S}$. Despite forming a massive and conspicuous seafloor expression, these features have received little attention in previous literature with regards to the tectonic evolution of the MRC. Likewise, the boundary between the Emerald and Solander basins is inferred to occur here at $\sim 51^{\circ}\text{S}$, yet details of this transition are rarely discussed.

We propose that the boundary between the Solander and Emerald basins represents a major change in the tectonic evolution of the AUS-PAC plate boundary. Key evidence derives from regional potential field data, which shows a sharp increase in the Bouguer gravity anomaly (McCubbine et al., 2017) from north to south (Figure 10). Bouguer gravity anomaly values south of $\sim 51.5^{\circ}\text{S}$ are similar to those observed on the incoming oceanic Australian Plate and typical of regional oceanic lithosphere. To the north, Bouguer gravity anomaly values are slightly reduced and consistent with thinned continental domains found elsewhere in Zealandia, such as Bounty Trough. A transfer zone between the oceanic crust in the Emerald Basin and the stretched continental crust of the Solander Basin could explain the step in Bouguer gravity anomaly between

the two basins. Furthermore, plate reconstructions place the Resolution Ridge System against Campbell Plateau just south of these blocky structures at ~45 Ma (Cande & Stock, 2004). All of these lines of evidence argue that the NE-SW oriented COT along Campbell Plateau turns 90° at ~51.5°S and intersects the MRC. This southern COT (and boundary between Solander and Emerald basins and Eocene junction between the Challenger and Campbell plateaus) implies that the upper Pacific Plate contains continental lithosphere along the entire Puysegur segment and that the MSC did not propagate northward to the Puysegur margin. Deep Sea Drilling Project (DSDP) site 279 recovered oceanic basalt near the McDougall Ridge in the Emerald Basin (Figure 10), confirming the presence of oceanic lithosphere southwest of our proposed COT. The large blocky highs along the southern COT likely formed as a result of the complicated transition from focused seafloor spreading in the Emerald Basin to distributed continental rifting and inherited basement structure from the junction of the Campbell and Challenger plateaus. Strong changes in the nature of tectonic deformation across the COT could have caused a non-linear decrease in the amount of extension from rifting in Solander Basin compared to efficient seafloor spreading at the MSC in the Emerald Basin. Consequently, variations in properties of the lithosphere across the southern COT signify an important inherited structure, which likely influenced subduction initiation and segmentation of the AUS-PAC plate boundary over time.

6.2 Origin of Puysegur Ridge

We propose that the Puysegur Ridge (east of the strike-slip Puysegur Fault) is composed entirely of continental lithosphere; therefore, it may not be a natural extension of the Hjort, Macquarie, and McDougall oceanic ridges along the MRC. These other ridges are thought to be the result of broader transpression across the AUS-PAC plate boundary since the Pliocene (e.g., Massell et al., 2000). There is good evidence that the regional Pliocene-recent transpressional stresses have caused slight uplift of Puysegur Ridge; however, its earlier buoyancy and paleotopography during strike-slip and subduction initiation were inherited from the continental rifting phase.

Rift symmetry (or lack thereof) is commonly used to infer the primary stress conditions and resulting strain patterns during extension of continental lithosphere (Lister et al., 1986). Asymmetric rifts are not uncommon and typically involve one or more basin-wide detachment faults (e.g., Axen & Bartley, 1997). It is thought that simple-shear is the primary strain regime to invoke rift asymmetry because it involves rotation, which can lead to fault-bounded rider crustal blocks exhuming along a weak rolling-hinge detachment. Though we have not imaged a deep detachment fault beneath the Solander Basin, we believe that a rolling-hinge model can explain the rift architecture along the SISIE-2 (northern) MCS/OBS profile, which is highly asymmetric. Most crustal thinning occurred just west of Campbell Plateau, where landward-dipping normal faults offset tilted high-relief crustal blocks. In contrast, along SISIE-1 the pure-shear stretching model involves symmetric brittle faulting in the upper crust accompanied by uniform ductile flow in the weak lower crust. The presence of both west and east-dipping normal faults and less asymmetry on SISIE-1 suggest that the southern rift may have involved a combination of simple and pure-shear deformation. Additionally, the relatively lower basement relief displayed on crustal faults along SISIE-1 may reflect a polyphase history of multiple fault generations, wherein younger faults offset older faults and act to flatten the crust over time (McDermott & Reston, 2015).

Our proposed evolution of continental rifting in the Solander Basin can explain the overall basin architecture and the origin of Puysegur Ridge. Regardless of simple or pure shear stretching, our β -value distributions confirm that crustal thinning was highly asymmetric on both profiles,

with the thinnest ($\beta \sim 4$) crust located adjacent to the Campbell Plateau (Figure S1). Overall, the asymmetry of rifting processes focused thinning in eastern Solander Basin and gradually less stretching towards the west. Strikingly, the crust at Puysegur Ridge shows little to no thinning ($\beta < 2$) and has no sedimentary cover. Pliocene-recent shortening did not significantly thicken the crust here, because the imaged throw across basement faults is minor (few 100s of meters) (Figure 6). This result implies that Puysegur Ridge was a prominent local topographic high at the end of the rifting phase, and it has persisted as an important inherited structural feature along the AUS-PAC boundary subsequently.

Our interpretation of the origin of Puysegur Ridge has two major implications. First, the minimally thinned crust at Puysegur Ridge was likely proximal and/or continuous with unstretched Challenger Plateau crust during the late stages of rifting. Hence there is not a missing conjugate to the Solander Basin. This finding refutes the idea that a large section of oceanic lithosphere was produced by symmetric seafloor spreading west of Solander Basin, and that this missing conjugate seafloor was later subducted beneath South Island (e.g., Sutherland et al., 2000). The locus of rifting and strike-slip along the Puysegur margin must be accounted for in future plate reconstructions of Zealandia. Second, Puysegur Ridge was already a significant topographic high during and after continental rifting. This result is important because it implies that the leading edge of the Pacific Plate during convergence was thick and low-density continental crust, which suggests buoyancy was a key controlling factor for the initiation of subduction at Puysegur (Gurnis et al., 2019). Furthermore, the uplifted Puysegur Ridge likely acted as a barrier trapping most sedimentary routing systems and shielding the Solander Basin from the Antarctic Circumpolar Current (ACC), resulting in the thick basin fill observed today (e.g., Patel et al., 2020).

6.3 Cessation of the Solander Basin Rift and Developing Strike-Slip Movement

The timing involved in the transition from rifting to strike-slip motion along the Puysegur margin is mostly constrained by magnetic anomalies in the Southeast Tasman Basin and farther south in the Emerald Basin (Keller, 2004; Cande & Stock, 2004). Plate reconstructions show that seafloor spreading along the MSC was relatively orthogonal between ~ 40 -30 Ma (Keller, 2004). Southeastward migration of the stage rotation pole between 30-25 Ma, relative to the Pacific plate, eventually established a new phase of dominantly right-lateral strike-slip motion along the entire AUS-PAC plate boundary. Spreading segments became shorter and fracture zones curved, eventually linking and forming the MRC. Based on proximity to the rotation pole, plate motions suggest that the transition to strike-slip may have started in the north and slowly propagated southward.

Our results indicate that strike-slip motion along the Puysegur margin localized westward of the extensional structures developed during continental rifting. This result may be surprising given that the thinnest crust and focus of rifting was adjacent to Campbell Plateau, approximately 60-90 km east of the eventual location of strike slip strain localization. Moreover, our β distributions (Figure S1) reveal that strike-slip localized within relatively thicker and apparently stronger crust of the adjacent Challenger Plateau, which was located to the west of Puysegur Ridge. We speculate that strike-slip localization outside the rift zone at the Puysegur Margin may have been preferred due to alignment with the developing strike-slip along the MRC plate boundary in the south, which was located farther west than the locus of rifting (Keller, 2004). In addition, igneous intrusions in the thinned continental crust and cooling of the uppermost mantle of the rift zone may have homogenized and strengthened the lithosphere, thus resisting strain localization within the Solander Basin after ~ 25 Ma. Regardless of the mechanisms, strike-slip strain localization west of the rift zone effectively severed the extended crust domain and abandoned it

as a failed rift basin on the Pacific Plate. Consequently, the Solander Basin rift never achieved full continental breakup and seafloor spreading due to changing plate motions which shifted the locus of deformation.

By the end of the Oligocene, strike-slip was the dominant style of plate motion along the entire AUS-PAC plate boundary. Although estimates vary, it is well accepted that at least 400 km of dextral motion (e.g., Sutherland, 1999) has occurred on the Alpine Fault (and presumably the MRC) since ~25 Ma. Thus, the question remains, what happened to the lithosphere west of the dextral strike-slip Puysegur Fault Zone? An older accepted view of the tectonic history assumes that symmetric seafloor spreading between the Campbell Plateau to the east and Challenger Plateau to the west produced a wide swath of oceanic lithosphere. In this scenario, the eastern flank of the oceanic rift now lies beneath the Solander Basin, while the conjugate western flank subducted beneath South Island (Sutherland, 1995; Sutherland et al., 2000; Lebrun et al., 2003; Hayes et al., 2009).

Closer to South Island, the location of Oligocene strike-slip development and eventual connection between the Puysegur and Alpine faults remain unclear. As noted earlier, strike-slip faulting clearly becomes more distributed north of ~48°S and from east to west the structures curve counterclockwise to the northwest in a left-stepping fashion (Lamarche & Lebrun, 2000). Many plate reconstructions ignore this complex zone of deformation along the South Island continental shelf and perform rigid plate reconstructions along the present-day Alpine Fault. As a result, these rigid reconstructions often have significant overlap between the Challenger and Campbell plateaus and fail to align the geological terranes exposed on the South Island (e.g., Lamb et al., 2016). In particular, reconstructing the location of the Fiordland block and estimating the distribution of strain within Fiordland has been problematic.

As an alternative, Lebrun et al. (2003) proposed that the proto-strike-slip plate boundary developed on the Moonlight Fault System (MFS) located to the east of Fiordland. The kinematic reconstructions of Lebrun et al. (2003) translate Fiordland ~30 km to the northeast between the Oligocene and Middle Miocene, supported by geometric observations of onshore terranes, and geological evidence of ~25-30 km of dextral strike-slip across the MFS (Norris and Turnbull, 1993; Uruski, 1992 – see Lebrun 2003). We prefer the model of Lebrun et al. (2003), where the Fiordland block was mechanically attached to the Australian Plate initially. This scenario would imply that the dextral shear zone offset Puysegur Ridge from relatively unstretched continental lithosphere of the eastern Challenger Plateau. The eventual westward migration of strain from the MFS to the Balleny, Alpine, and other faults in a left-stepping fashion may have been associated with the “docking” of the Fiordland block. Increased northward convergence of relatively thick continental lithosphere over time would likely have induced a modest collision zone within and behind the Fiordland block. Evidence for uplift along northern Puysegur Bank has been well documented (Lamarche & Lebrun, 2000; Sutherland et al., 2006) and includes tilted and truncated beds with recovered dredge samples containing pollen and spores from a coastal environment. Detailed thermochronology data constrain the onset of rapid exhumation at ~25 Ma starting in southwestern Fiordland (House et al., 2002; Sutherland et al., 2009). Recent structural analyses of Fiordland rocks reveal a distinct phase of transpression with mixed dextral strike-slip and oblique shearing from ~25-10 Ma (Klepeis et al., 2019). Additionally, chronostratigraphic analyses of Solander Basin show that the sediment accumulation rates spiked in the Middle Miocene, suggesting that Fiordland orogenesis became a significant sediment source at this time. Based on these accounts, it is likely that early phases of uplift in Fiordland and offshore Puysegur Bank are

related to continent collision and the formation of a transpressional relay zone between the MFS and the Alpine Fault as convergence along the plate boundary increased over time.

6.4 Geodynamic Setting of Subduction Initiation

Earlier phases of continental rifting and strike-slip activity along the Puysegur margin created the necessary conditions for subduction initiation. New seismic images from the SISIE survey have revealed that the Solander Basin basement consists entirely of extended continental crust formed during Eocene-Oligocene extension (Gurnis et al., 2019; this study), not oceanic crust as previously thought. Subsequent strike-slip deformation developed west of the rift zone, either because of preferable geometric linkage to the MRC farther south, or because the lithosphere in the rift zone, albeit extended and magmatically intruded, was relatively strong. Therefore, continental rifting alone did not create strongly favorable conditions to facilitate underthrusting, and convergence across the margin at ~30 Ma would probably not have advanced to subduction initiation. Instead, the ensuing episode of dextral strike-slip caused several events which promoted favorable conditions for subduction initiation: (1) Continental collision between Puysegur Bank and South Island formed a restraining bend with left-stepping, right-lateral faults between the MFS and Alpine fault; (2) trailing oceanic lithosphere created on the Australian side of the MSC was translated northward by the MRC and juxtaposed with Fiordland to the north and thick continental crust of Puysegur Ridge to the east; (3) gradual counterclockwise rotation of the Balleny relay zone faults to a NW-SE orientation became favorably oriented to accommodate more compression and shortening; (4) erosion of the Fiordland mountains and the establishment of sediment routing systems transported sediments across the margin along the proto-trench and therefore could have hosted fluids to weaken the nascent subduction interface.

These favorable geodynamic conditions culminated in subduction initiation in the Middle Miocene near present-day Puysegur Bank. The existence of weakening mechanisms and progressively increased plate convergence ultimately allowed subduction to initiate as oceanic lithosphere was forcibly underthrust beneath the continental collision zone. The nascent subduction thrust successively developed and spread to the south along the Puysegur margin over time. Our preferred model of subduction initiation at a restraining bend is in good agreement with models put forth by Lamarche & Lebrun (2000) and Lebrun et al. (2003), which is remarkable given the lack of deep-penetrating seismic data along the margin before the SISIE survey. Other prevailing models of subduction initiation at Puysegur including at an oceanic fracture zone (Collot et al., 1995) are not consistent with our findings.

Ongoing debate regarding the different subduction initiation models mostly arises from outstanding questions regarding the nature of the lithosphere between the Puysegur Trench and Puysegur Fault, and whether underthrusting took place on an existing fault that rotated over time or on a new fault that broke at a shallower angle. Up to this point, it was thought that most of the Puysegur subduction zone is intraoceanic, i.e. oceanic lithosphere exists to the west and east of the Puysegur Fault. Here we have established that the eastern flank of Puysegur Ridge is composed of extended continental crust, and we observe a major seismic velocity contrast across the Puysegur Fault. Therefore, it is likely that the lithosphere between the Puysegur trench and ridge is oceanic in nature and has been juxtaposed with the Solander Basin rift domain by the Puysegur Fault. Collot et al. (1995) suggested that a lithospheric density contrast occurs across Puysegur Ridge, since bathymetry data show that the western flank is more than 1 km deeper than the eastern flank in some places. Hatherton (1967) early on recognized a strong positive magnetic anomaly associated with the Puysegur Ridge and attributed it to uplifted oceanic lithosphere. Shipboard magnetic anomaly data from MGL1803 reveal that magnetic anomaly is typically higher on the

western side of Puysegur Ridge and support a continental-oceanic juxtaposition (Figure 10). Additionally, although few and sparse, dredge samples from the western flank of Puysegur Ridge and southern Puysegur Bank found altered cobbles of basalt, diabase, and gabbro with mid-ocean ridge basalt and ocean-island basalt affinities (Figure 10; Mortimer, 1994), consistent with the geochemistry of other igneous rocks sampled along the MRC. Recent work by Hightower et al. (2019) performed 3D Bayesian inversion of gravity data and confirmed the presence of high-density bodies along the western flank of Puysegur Ridge. Lamarche and Lebrun (2000) proposed that the lithosphere between the Puysegur Fault and Puysegur Trench forms an oceanic tectonic sliver, which moves independently of the Australian and Pacific plates.

Our findings support the existence of an oceanic sliver, which was likely captured during the subduction initiation process. This sliver appears to now behave as a strain-partitioned, forearc sliver observed in many subduction zones (e.g., Fitch, 1972; Martin et al., 2010; 2014). We speculate that subduction started primarily at the COT but a piece of the initially downgoing oceanic lithosphere became scraped off and detached in the process. This scenario would imply that a new plate boundary fault formed west of the COT. It is possible that the wedge shape of the sliver could reflect growth through time, and that fracture zones may have progressively linked with the developing subduction interface resulting in the capture of oceanic lithosphere fragments to the sliver. Puysegur Bank and Puysegur Ridge are exciting targets for future ocean drilling expeditions and passive ocean-bottom seismometer deployments that are needed to verify the tectonic origin of the sliver and uncover details of the subduction initiation process along the margin.

6.5 Reconciliation with Plate Reconstructions

Until we gathered new regional seismic images, there was a debate about the nature of the Australian Plate crust that first entered the Puysegur subduction zone and speculations about the present-day location of this missing lithosphere (Sutherland, 1995; Sutherland et al., 2000; Lebrun et al., 2003; Sutherland et al., 2006). The amount of subducted material has been estimated using plate reconstructions constrained by magnetic isochrons and the present-day location of the slab from earthquake seismicity data (Sutherland et al., 2000). Using best-fitting plate reconstruction models, it was estimated that in total $\sim 9 \times 10^4$ km² of oceanic lithosphere has disappeared beneath South Island since subduction initiated (Sutherland et al., 2000). However, Sutherland et al. (2000) discovered that a slab reconstruction based on the geometry of deep seismicity can account for only $\sim 6 \times 10^4$ km² of underthrust seafloor, leaving at least $\sim 3 \times 10^4$ km² Australian Plate crust missing in the reconstructions and undetected seismically. Sutherland et al. (2000) proposed that the missing lithosphere may be aseismic but still attached to the Challenger Plateau, and currently beneath the western edge of the Southern Alps. Alternatively, Lebrun et al. (2003) suggested that the aseismic lithosphere became detached and underplated beneath the South Island to explain the anomalous high-velocity zone beneath Fiordland in seismic tomography images (Eberhart-Phillips & Reyners, 2001; Reyners et al., 2002). As a new alternative, we propose instead that the mismatch in missing and underthrust seafloor likely arises from incorrect assumptions about the nature of the crust and plate boundary during the Eocene-Miocene between ~ 51 - 47° S.

To calculate the area of subducted oceanic lithosphere, Sutherland et al. (2000) and successive studies made the following assumptions: (1) a passive margin exists along the west edge of the Campbell Plateau from $\sim 47^\circ$ S to 55° S; (2) the Solander Basin contains Eocene-Miocene aged oceanic crust created by seafloor spreading along the MSC; (3) every passive margin formed by extension and every piece of oceanic lithosphere has a conjugate feature formed contemporaneously; and (4) Australian-Pacific plate motion since 45 Ma is known precisely. Our

results, however, support the following: (1) the western edge of Campbell Plateau instead represents a failed rift north of $\sim 51.5^{\circ}\text{S}$; (2) seafloor spreading was never active in the Solander Basin; (3) continental crust in the Solander Basin has been asymmetrically extended and does not have a missing conjugate; and (4) slightly less extension occurred in the Solander Basin ($\sim 47\text{--}75$ km) than what is predicted by fitting rotation poles using magnetic anomalies from the Emerald Basin. Thus, we alternatively suggest that the missing aseismic lithosphere does not exist and is merely an artifact of plate reconstruction assumptions. With these assumptions, previous plate reconstructions suggested that the first crust to subduct was young and hot oceanic lithosphere created at the MSC at a similar latitude as the proto Puysegur Trench. Conversely, in our proposed model, the first material involved in subduction would have actually been oceanic lithosphere created at the MSC south of $\sim 51^{\circ}\text{S}$. In this scenario, the underthrusting oceanic lithosphere would be at least ~ 10 million years old and therefore inherently negatively buoyant relative to continental lithosphere and thus less resistant to subduction initiation (Cloos, 1993; Leng and Gurnis, 2015).

7. Summary of Revised Tectonic Evolution

We propose an updated Cenozoic tectonic evolution of the Australian-Pacific plate boundary from new active-source seismic constraints along the Puysegur margin (Figure 11). Throughout the late Cretaceous-Paleocene, Zealandia continued to drift away from Antarctica and Australia by the creation of new oceanic lithosphere along the Tasman Sea and Antarctic-Pacific spreading centers. In the Early Eocene, a dramatic change in plate motions caused the cessation of seafloor spreading in the Tasman Sea around ~ 53 Ma. Around ~ 45 Ma, a new phase of seafloor spreading was established along the Macquarie Spreading Center, which defined the proto Australian-Pacific plate boundary and propagated from south to north. The MSC initiated as an intraoceanic rift and quickly proceeded to seafloor spreading in the Macquarie Basin, accommodating east-west AUS-PAC extension. As the northern tip of the MSC approached the Campbell Plateau, the rift reactivated structures of the Cretaceous COT west of Campbell Plateau. This process included rafting several narrow blocks of continental crust off the plateau, which now form the continental domain of the Resolution Ridge System on the present-day Australian Plate. However, near 51.5°S the MSC met the junction of the Challenger and Campbell plateaus and was not able to propagate farther north into the thick continental lithosphere. From the middle Eocene to early Oligocene and north of $\sim 51.5^{\circ}\text{S}$, nearly orthogonal plate movement was accommodated by distributed tectonic extension that thinned the crust and created the Solander Basin. This episode of rifting involved large-offset normal faults concurrent with syn-rift sediment flux and rift-related volcanism and magmatic underplating. Crustal stretching was highly asymmetric and produced the thinnest crust adjacent to the western edge of Campbell Plateau, which aligned with the Eocene rifted margin farther south. Farther south at this time, seafloor spreading was active along the MSC accreting new oceanic lithosphere in a symmetric fashion.

Relative AUS-PAC plate motion became increasingly oblique when the rotation pole migrated southward during the late Oligocene to early Miocene, resulting in short and oblique spreading centers separated by long-offset fracture zones along the MSC. Curved fracture zones in the Tasman Sea are evidence that ~ 25 Ma motion along the AUS-PAC plate boundary was dominantly dextral strike-slip as fracture zones linked and formed the MRC. However, along the Puysegur margin, strike-slip localized $\sim 70\text{--}100$ km west of the rift axis in relatively unstretched crust, possibly to better align with strike-slip motion along the MRC to the south. This reorganization effectively severed the zone of thinned continental crust and preserved the Solander Basin as a failed rift on the Pacific Plate. The new dextral strike-slip boundary propagated northward, initially along the Hauroko and Moonlight Fault System east of Fiordland. Strike-slip

motion translated relatively thick continental lithosphere of the eastern Challenger Plateau and trailing Australian oceanic lithosphere northward. Docking of the Fiordland block in southwestern South Island led to a new phase of dextral transpression and uplift in Fiordland and Puysegur Bank. This stage of transpression (~25-16 Ma) created new faults that formed in a left-stepping, right-lateral geometry, forming a transpressional relay zone between the MFS and the developing Alpine Fault to the west. Strike-slip motion along the MFS diminished as new faults rotated counterclockwise and accommodated increasing plate convergence. Strong compressional stresses produced distributed dextral shear across the relay and sparked the initial orogenesis in Fiordland.

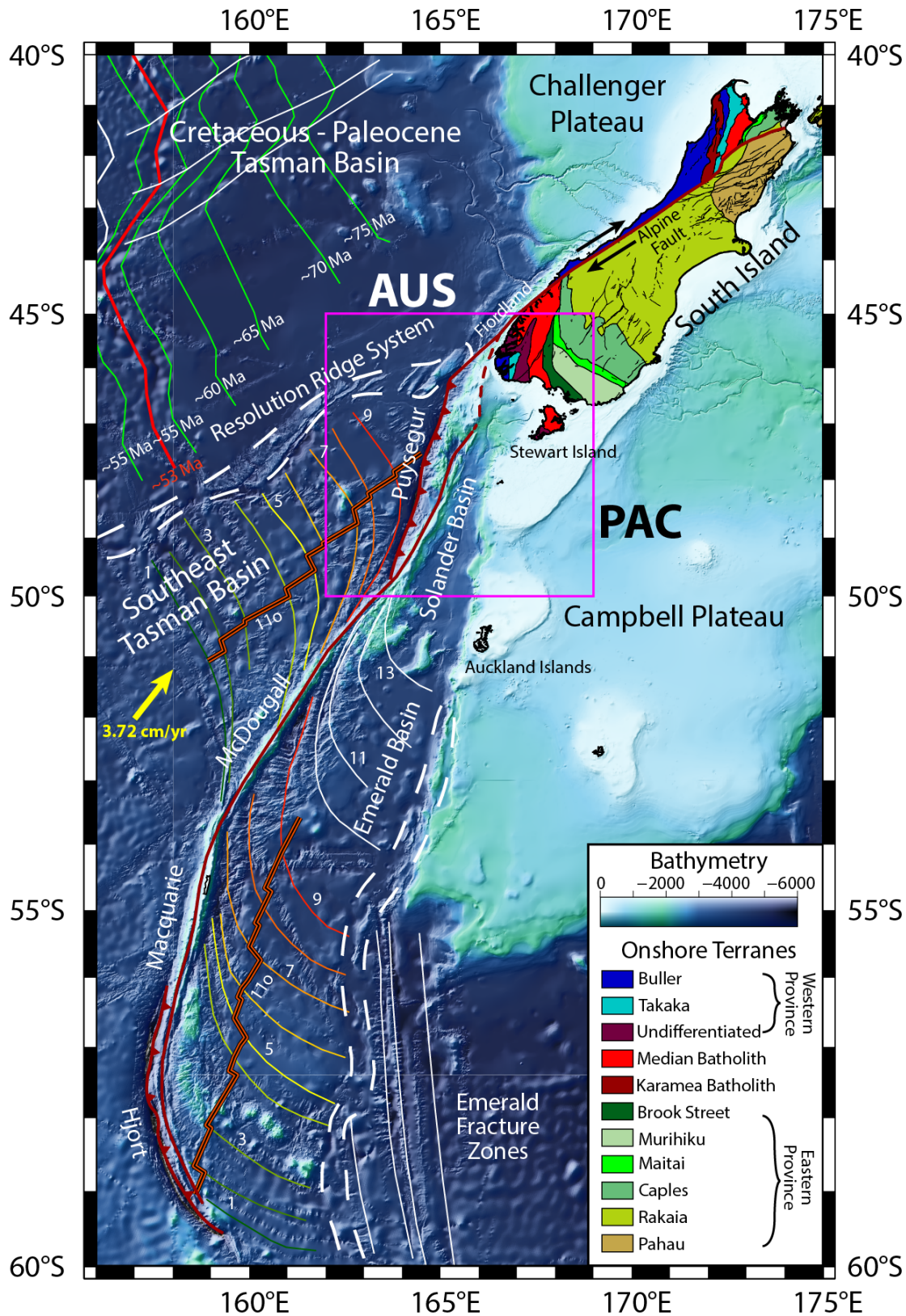
During the Middle Miocene, several inherited structures and weakening mechanisms facilitated subduction initiation at the Puysegur Trench. Thin and dense oceanic lithosphere forcibly underthrust beneath the thickened and uplifted continental relay zone near Puysegur Bank. Between ~16-7 Ma, the nascent trench lengthened along the strike of the plate boundary and captured detached fragments of Australian oceanic lithosphere, forming a tectonic sliver between the Puysegur Trench and Puysegur Fault. Dynamic stresses accompanying the subduction initiation process generated uplift and inversion of older rift faults in the upper plate and triggered distributed and rapid exhumation in Fiordland as the crust was propped up by the underthrusting slab. The creation of significant topography in the South Island led to erosion and enhanced sediment flux filling most of the Solander Basin low. Tectonic uplift throughout northern Puysegur margin ceased by ~8 Ma, possibly in response to deepening of the slab and hence an increase in its negative buoyancy. Since the Middle Miocene, the trench has lengthened and propagated southward through time, accommodating more AUS-PAC plate convergence and generating a wave of uplift along the southern Puysegur Ridge. The leading edge of the Resolution Ridge System collided with the overriding Pacific Plate at ~5 Ma, triggering renewed uplift in Fiordland and widespread thrusting along the southern continental shelf of the South Island. Quaternary adakitic volcanism at Solander Island represents the first signature of subduction-related volcanism, indicating that the Australian slab has reached appropriate depths and temperatures to undergo partial melting. Pliocene-Recent subsidence in southern Puysegur Bank, Snares Zone, and northern Puysegur Ridge, as well as normal faulting in northern Solander Basin, suggest that subduction may now be approaching a self-sustaining state along the northern Puysegur margin. In contrast, significant compressional stresses support the uplifted Puysegur Ridge and active reverse faulting in western Solander Basin, demonstrating that the southern margin is currently in a younger incipient stage of subduction.

Acknowledgments, Samples, and Data

We thank the captain, crew, and science party of the R/V *Marcus Langseth* for their efforts during the South Island Subduction Initiation Experiment. Thank you to Kelly Olsen, Andrew Gase, Justin Estep, and Dominik Kardell for guidance in seismic processing and invaluable feedback on seismic interpretations. Special thanks to the University of Texas Institute for Geophysics (UTIG) Marine Geology and Geophysics group for fruitful discussions which significantly improved this work. We are grateful to Mark Wiederspahn for his technical support and assistance with computational resources, and Marcy Davis and Dan Duncan for helping with multibeam and backscatter data gridding and visualization. The authors wish to acknowledge and thank the Paradigm University Grant Program of Emerson E&P Software for the use of Paradigm Echos for data processing in this project. The authors also wish to thank the Halliburton/Landmark University Grant program for the use of Decision Space Desktop and GeoProbe software used in the interpretation of this data. We thank IHS-Markit for a university

educational license for Kingdom software, provided to Caltech, for seismic data visualization and interpretation. Research in this manuscript was supported by the National Science Foundation through awards OCE-1654689 (UT Austin) and OCE-1654766 (Caltech). Uninterpreted and interpreted seismic images shown in this study can be found in the supporting information. Underway geophysical data from MGL1803 are available from the Rolling Deck Repository (<http://doi.org/10.7284/907966>). Raw and processed seismic data used in this study are available through the Marine Geoscience Data System (<http://doi.org/10.1594/IEDA/324659/>). This is UTIG Contribution #XXXX.

1234 **Figures and Figure Captions**



1235

Figure 1. Tectonic setting of the Australia (AUS) – Pacific (PAC) plate boundary south of New Zealand. Major strike-slip faults and trenches along the plate boundary are shown in red. Onshore faults shown in black. Pink box shows extent of Figure 2. Offshore bathymetry is plotted with artificial illumination from the northwest. Onshore geological terrane boundaries and mapped faults modified from GNS QMAP (Heron, 2018; <https://www.gns.cri.nz/Home/Our-Science/Land-and-Marine-Geoscience/Regional-Geology/Geological-Maps/1-250-000-Geological-Map-of-New-Zealand-QMAP>) and Cox and Sutherland (2007). Bathymetry data is publicly available from GEBCO (https://www.gebco.net/data_and_products/gridded_bathymetry_data/) and NIWA (<https://niwa.co.nz/our-science/oceans/bathymetry>). Isochrons of the Cretaceous-Paleocene Tasman Basin extracted from seafloor age database of Müller et al., (2008). Isochron 110 (~30.10 Ma) in the Southeast Tasman Basin from Keller (2004). Fracture zones in the Southeast Tasman Basin from Hayes et al. (2009) modified from Keller (2004) and Massell et al., (2000). Relative Australian Plate velocity from MORVEL (DeMets et al., 2010).

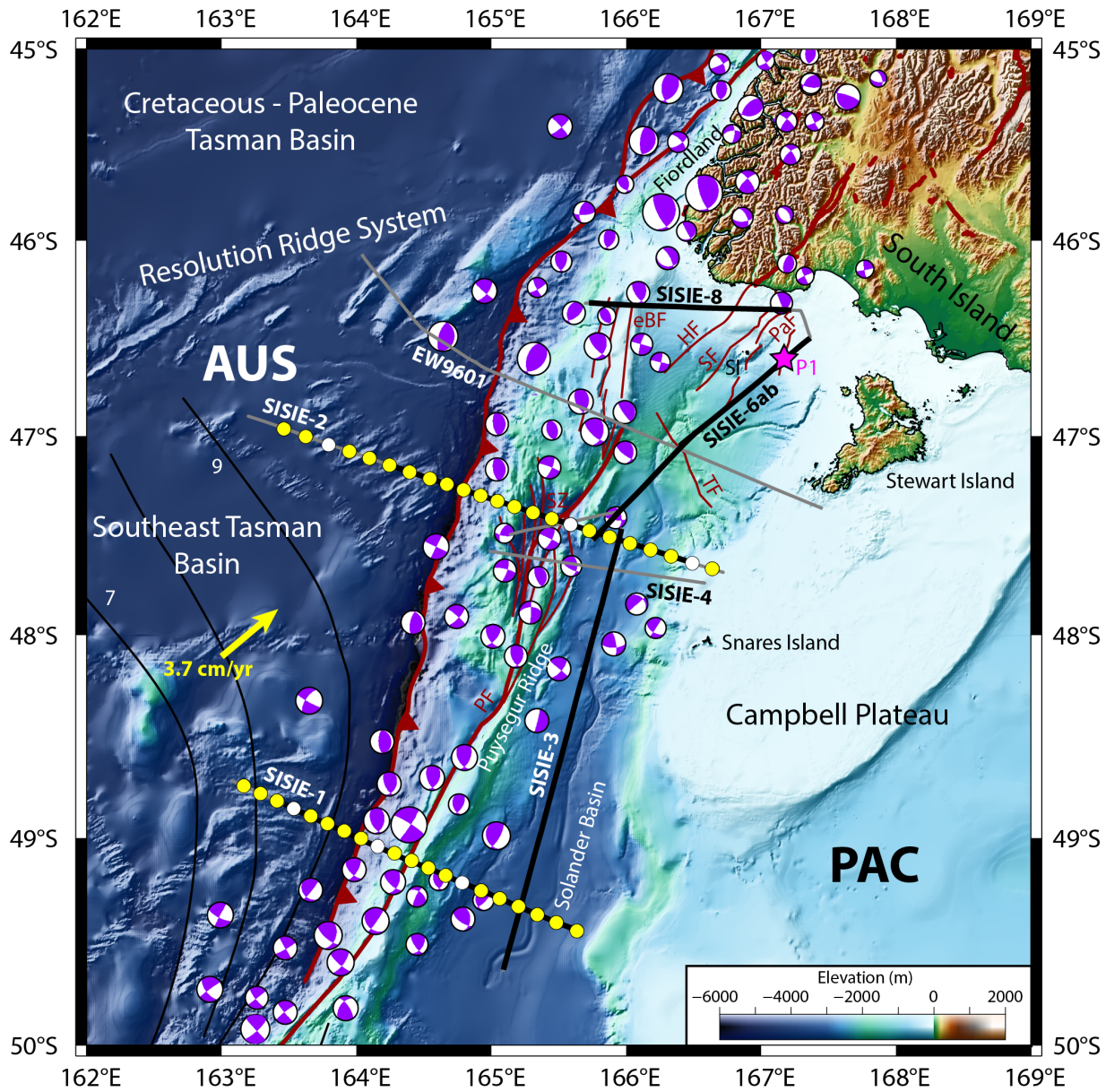


Figure 2. Elevation map showing major tectonic features of the Puysegur margin and the SISIE survey. Gray lines are the total extent of SISIE MCS lines, while thick black lines show the extent of the seismic lines shown in the figures of this paper. The location of the EW9601 seismic profile (Melhuish et al., 1999; Sutherland and Melhuish, 2000) is also shown in gray. Yellow circles represent successful OBS data used in analysis of this study; white circles represent OBS deployments with failed recovery or data recording. Pink star is the location of the Parara-1 borehole. Selected focal mechanisms from the global CMT (Dziewonski et al., 1981; Ekström et al., 2012) and GeoNet (<https://github.com/GeoNet/data/tree/master/moment-tensor>) earthquake catalogs. Offshore faults modified after Sutherland and Melhuish (2000) and Sutherland et al. (2006). SZ = Snares Zone; PB = Puysegur Bank; PF = Puysegur Fault; TF = Tauru Fault; PaF = Parara Fault; SF = Solander Fault; HF = Hauroko Fault; eBF = eastern Balleny Fault; SI = Solander Island.

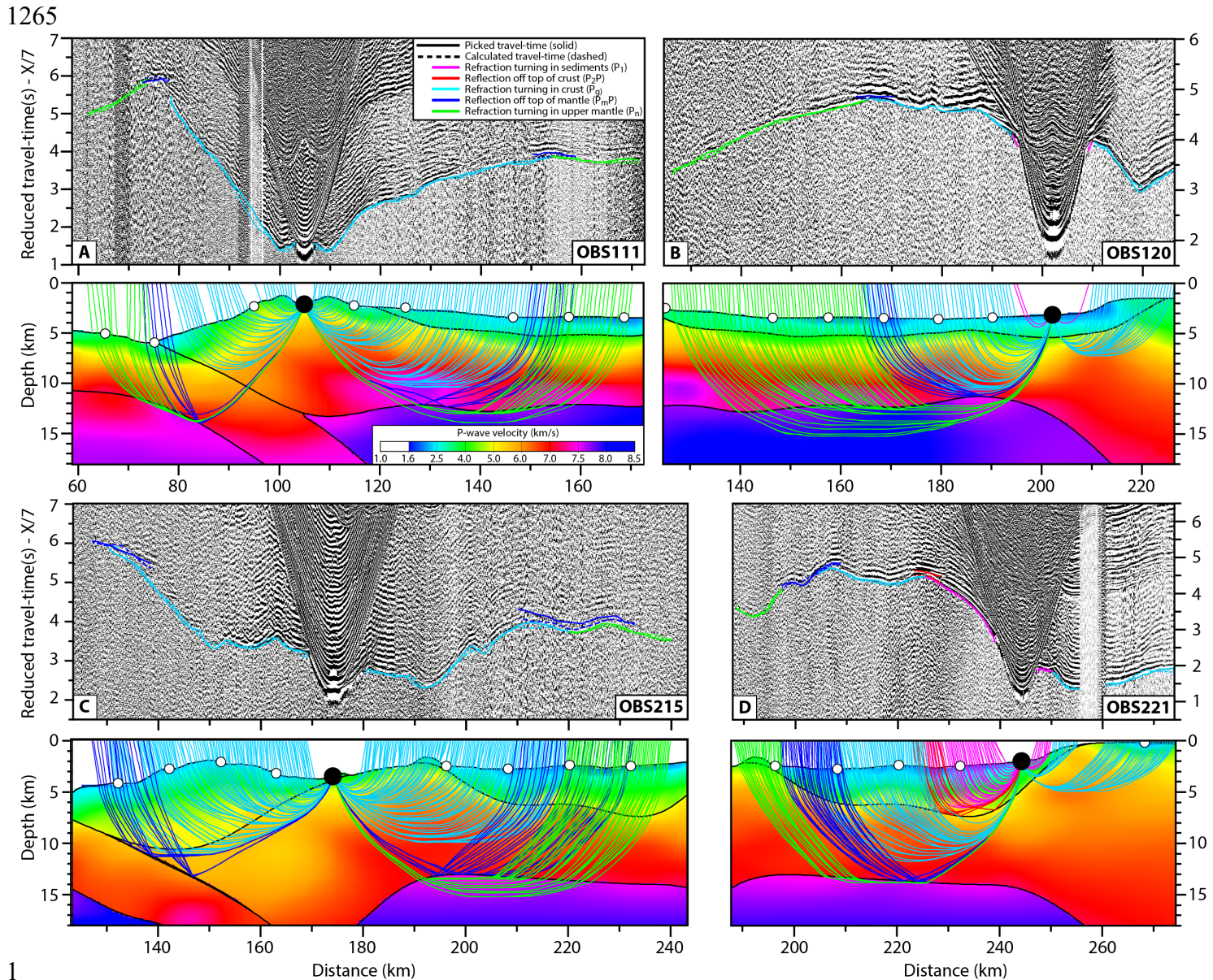


Figure 3. Interpreted OBS records and corresponding raytrace diagrams for instruments along SISIE-1 and SISIE-2. (a): Compressional waves for OBS111 at axis of Puysegur Ridge on SISIE-1. (b): Compressional waves for OBS120 at eastern Solander Basin on SISIE-1. (c): Compressional waves for OBS215 at the axial valley of the Snares Zone on SISIE-2. (d): Compressional waves for OBS221 at eastern Solander Basin on SISIE-2.

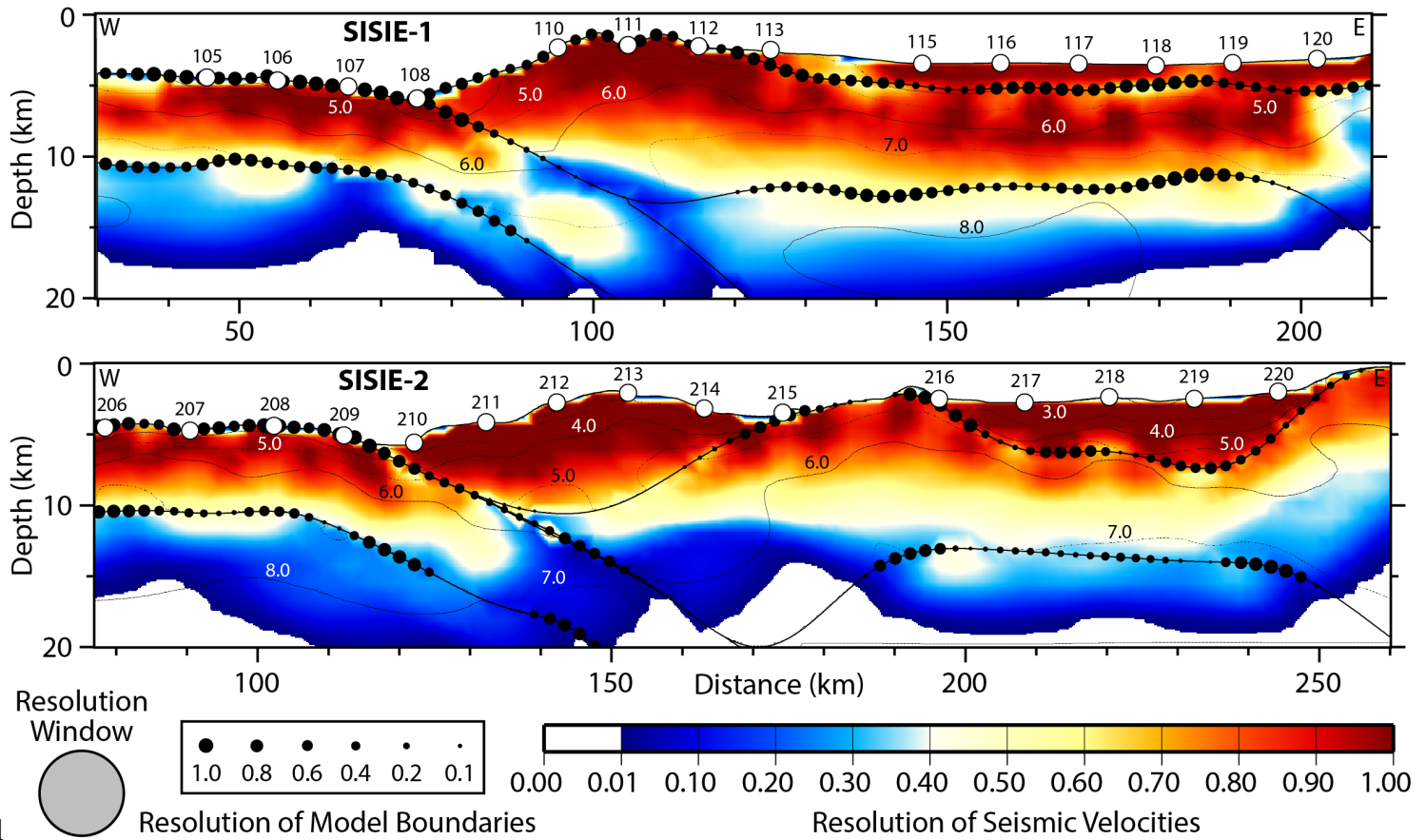


Figure 4. Resolution plots of final preferred tomography models for SISIE-1 and SISIE-2. Resolution obtained by applying the resolution matrix to a 12 km horizontal by 6 km vertical elliptical test structure. Resolution values of 1.0 are considered fully recovered, and we consider values >0.4 to be well recovered. Contours of P-wave velocity are at 1.0 km/s intervals.

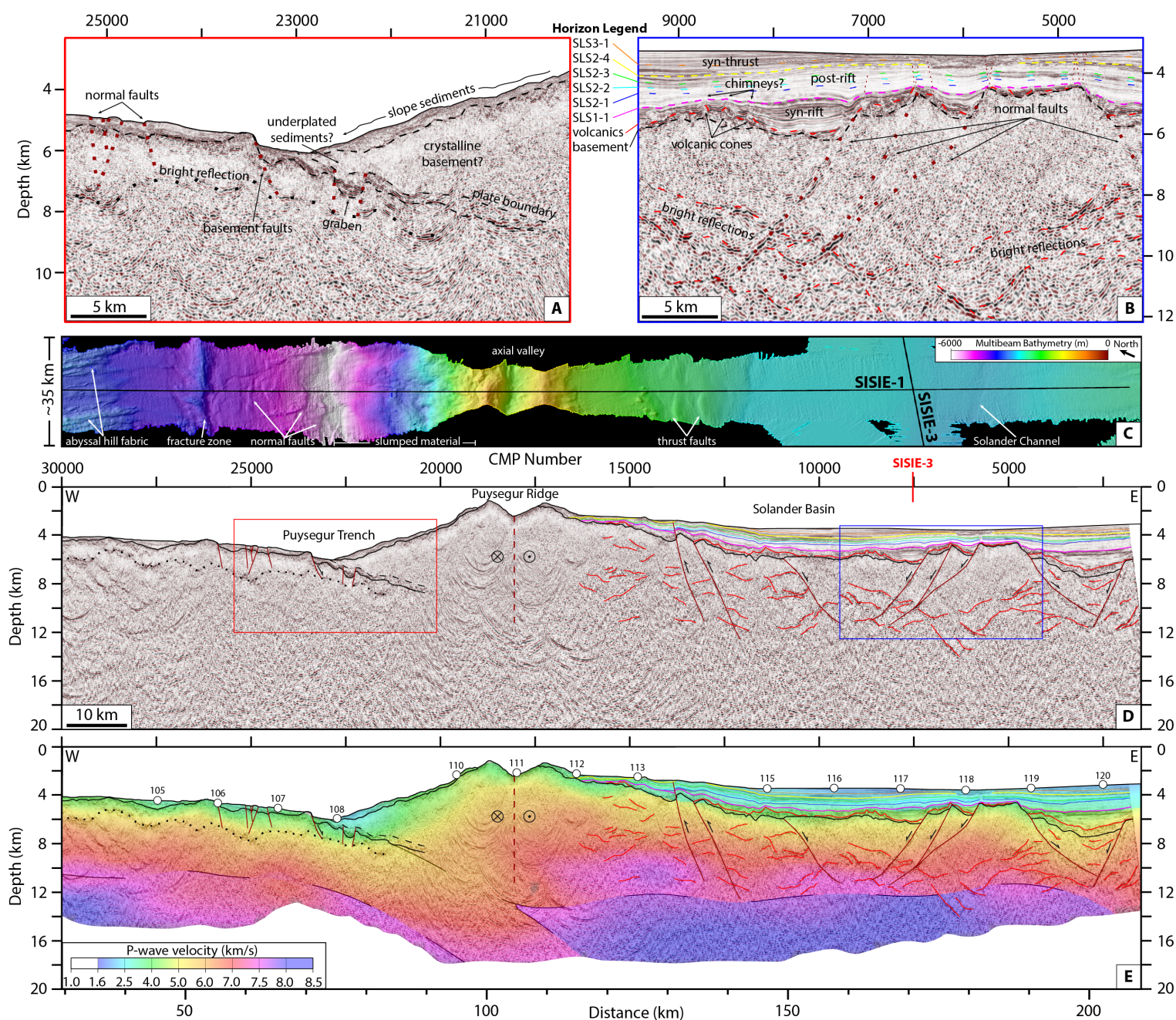


Figure 5. MCS, OBS, and bathymetry data along SISIE-1. (a): Zoom-in showing structure of the Puysegur Trench region (V.E. = 2x). (b): Zoom-in showing tectonostratigraphic interpretation, faulted crustal blocks, and intracrustal reflectivity within Solander Basin (V.E. = 2x). (c): Interpretation of shipboard multibeam bathymetry data. Bathymetry swath aligned with seismic profiles in d and e. (d): Pre-stack depth migrated MCS reflection image of the SISIE-1 profile (V.E. = 2x). Red lines outline bright intracrustal reflections. Black line is the top of basement reflection. (e): Compressional-wave (V_p) seismic velocity model overlain on MCS image in d. Velocity model is masked in regions with poor resolution and ray coverage.

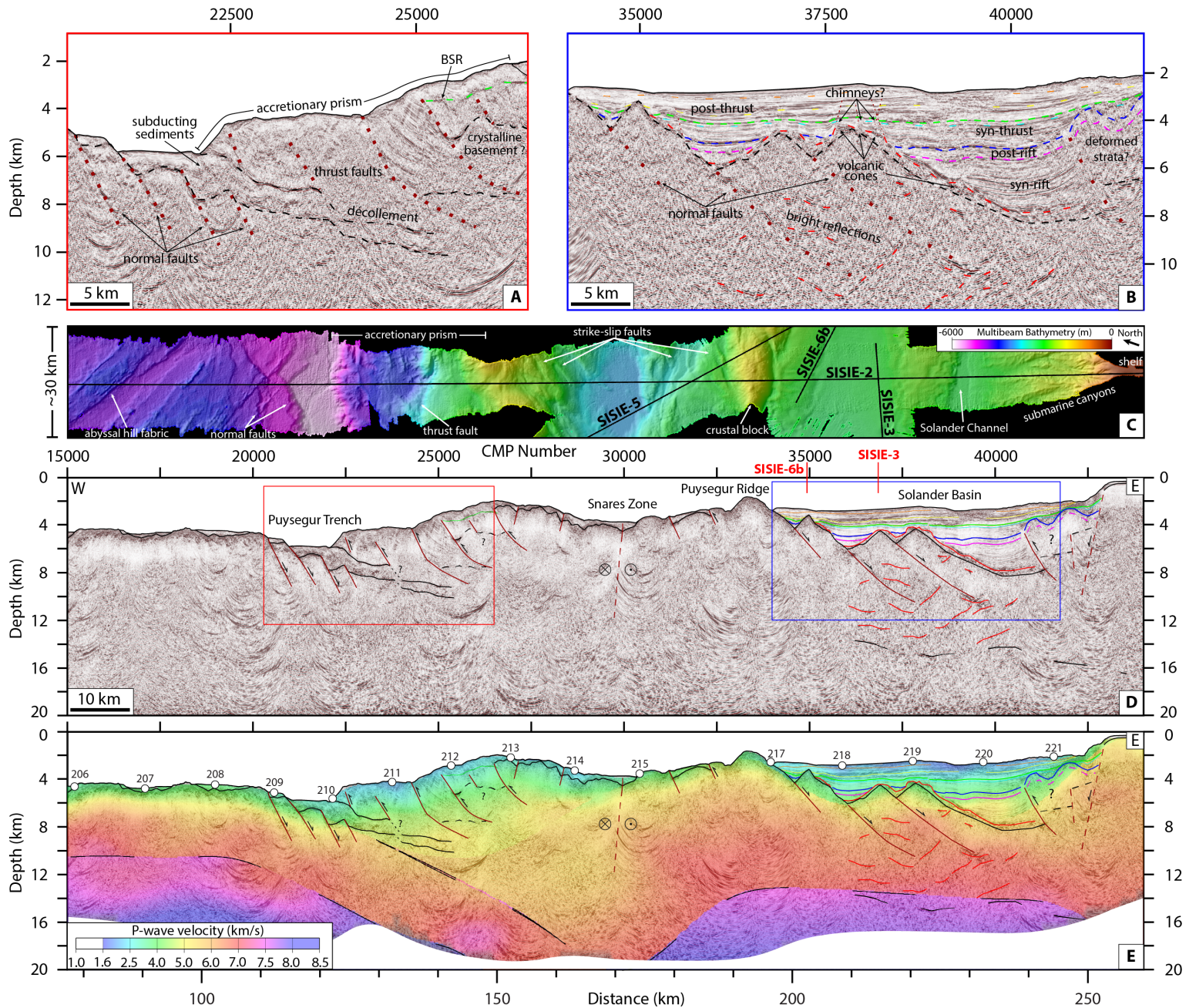


Figure 6. MCS, OBS, and bathymetry data along SISIE-2. (a): Zoom-in showing interpretation of the Puysegur Trench region (V.E. = 2x). (b): Zoom-in showing tectonostratigraphic interpretation, faulted crustal blocks, and intracrustal reflectivity within Solander Basin (V.E. = 2x). (c): Interpretation of shipboard multibeam bathymetry data. Bathymetry swath aligned with seismic profiles in d and e. (d): Pre-stack depth migrated MCS reflection image of the SISIE-2 profile (V.E. = 2x). Horizons and faults are dashed where uncertain. Red lines outline bright intracrustal reflections. Black line is the top of basement reflection. (e): Compressional-wave (V_p) seismic velocity model overlain on MCS image in d. Velocity model is masked in regions with poor resolution and ray coverage.

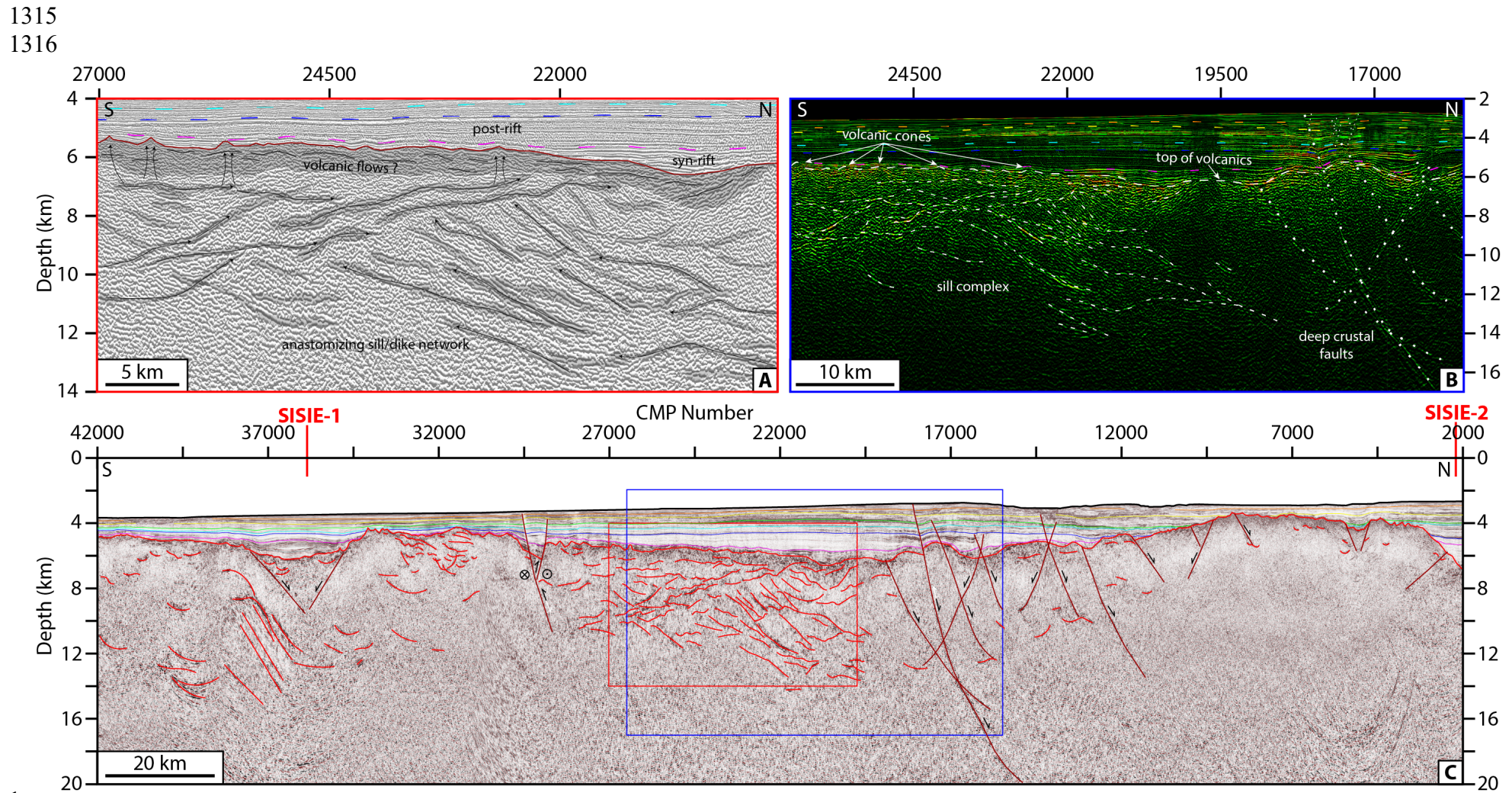


Figure 7. (a): Instantaneous phase seismic attribute image showing interpreted structure of igneous crustal features (V.E. = 2x). (b): Reflection strength seismic attribute image showing interpretations of igneous features and crustal faults (V.E. = 2x). (c): Pre-stack depth migrated MCS reflection image of the SISIE-3 profile (V.E. = 3x).

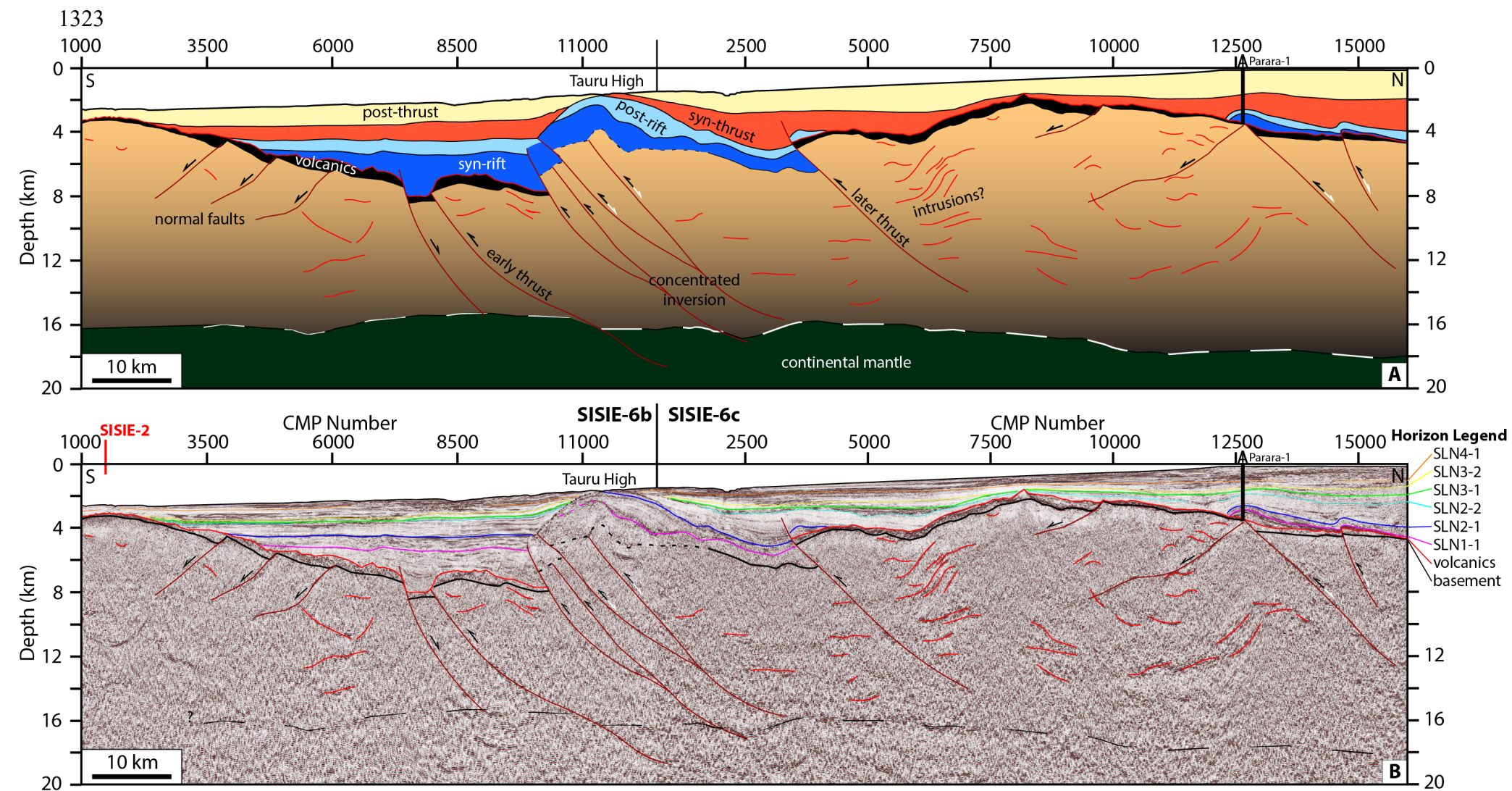


Figure 8. (a): Interpreted cartoon of crustal structure and tectonostratigraphic packages of the SISIE-6bc profile. (b): Pre-stack depth migrated MCS reflection image of the SISIE-6bc profile (V.E. = 2x). Horizons dashed where uncertain.

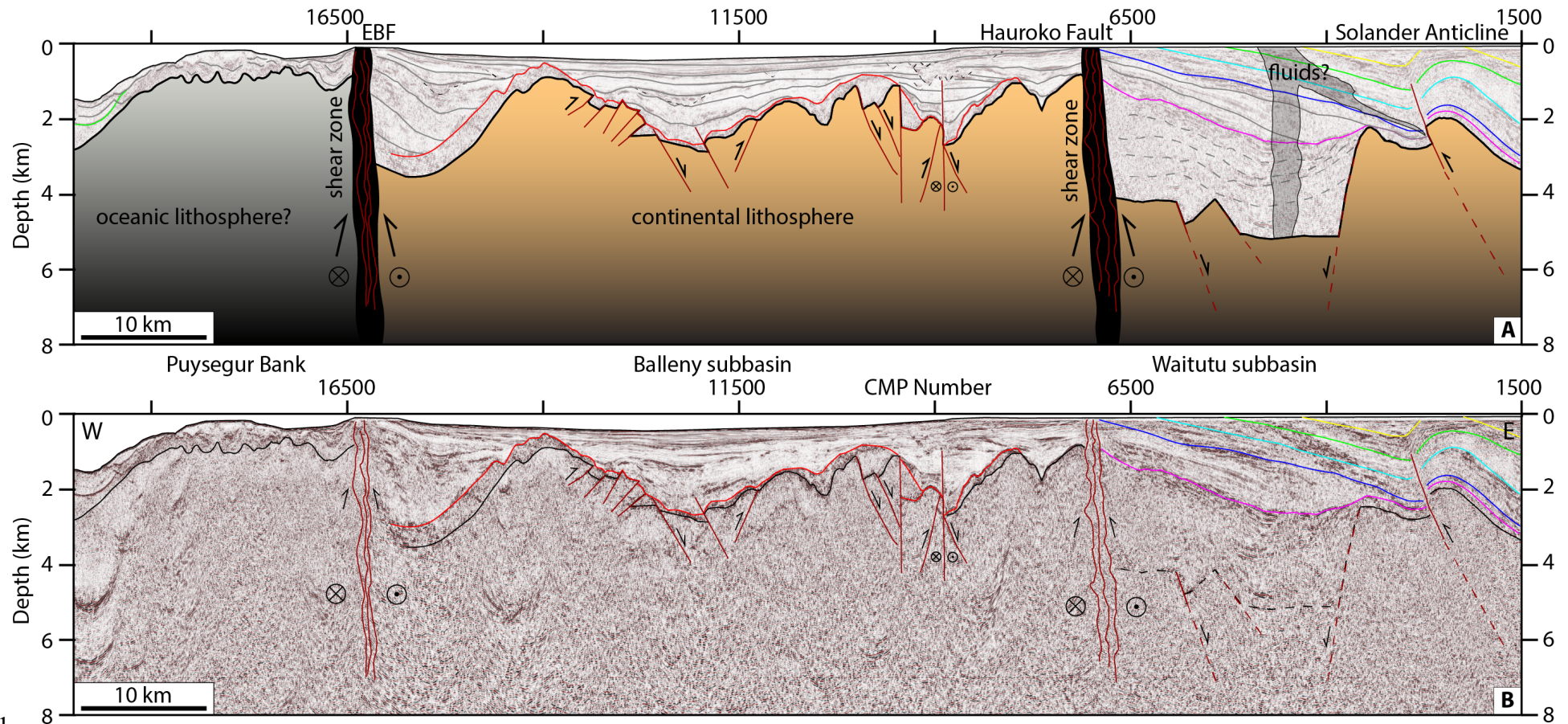


Figure 9. (a): Interpreted cartoon of crustal structure along the SISIE-8 profile. Continental and oceanic lithosphere are juxtaposed across the eastern Balleny Fault. (eBF). (b): Pre-stack depth migrated MCS reflection image of the SISIE-8 profile (V.E. = 3x).

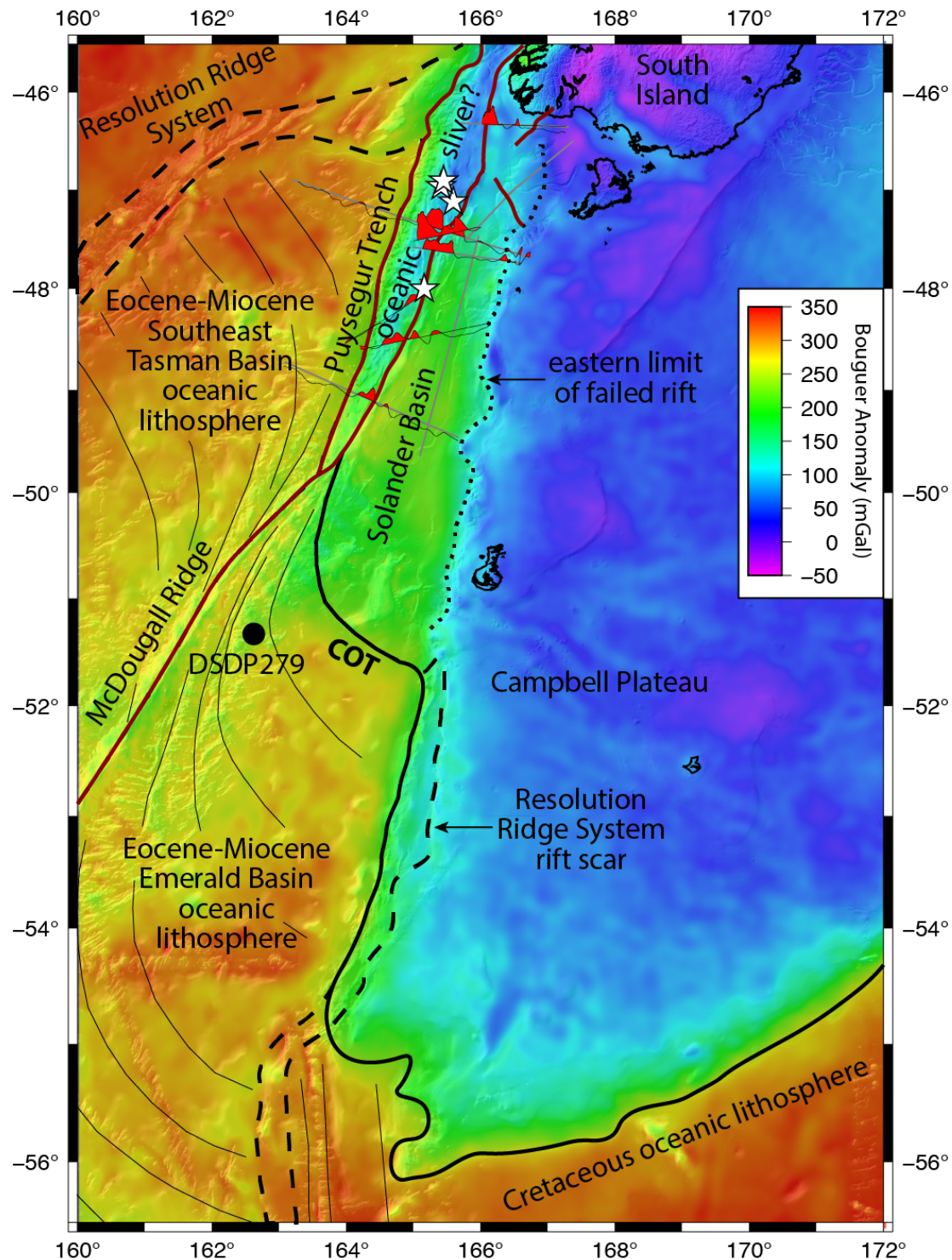
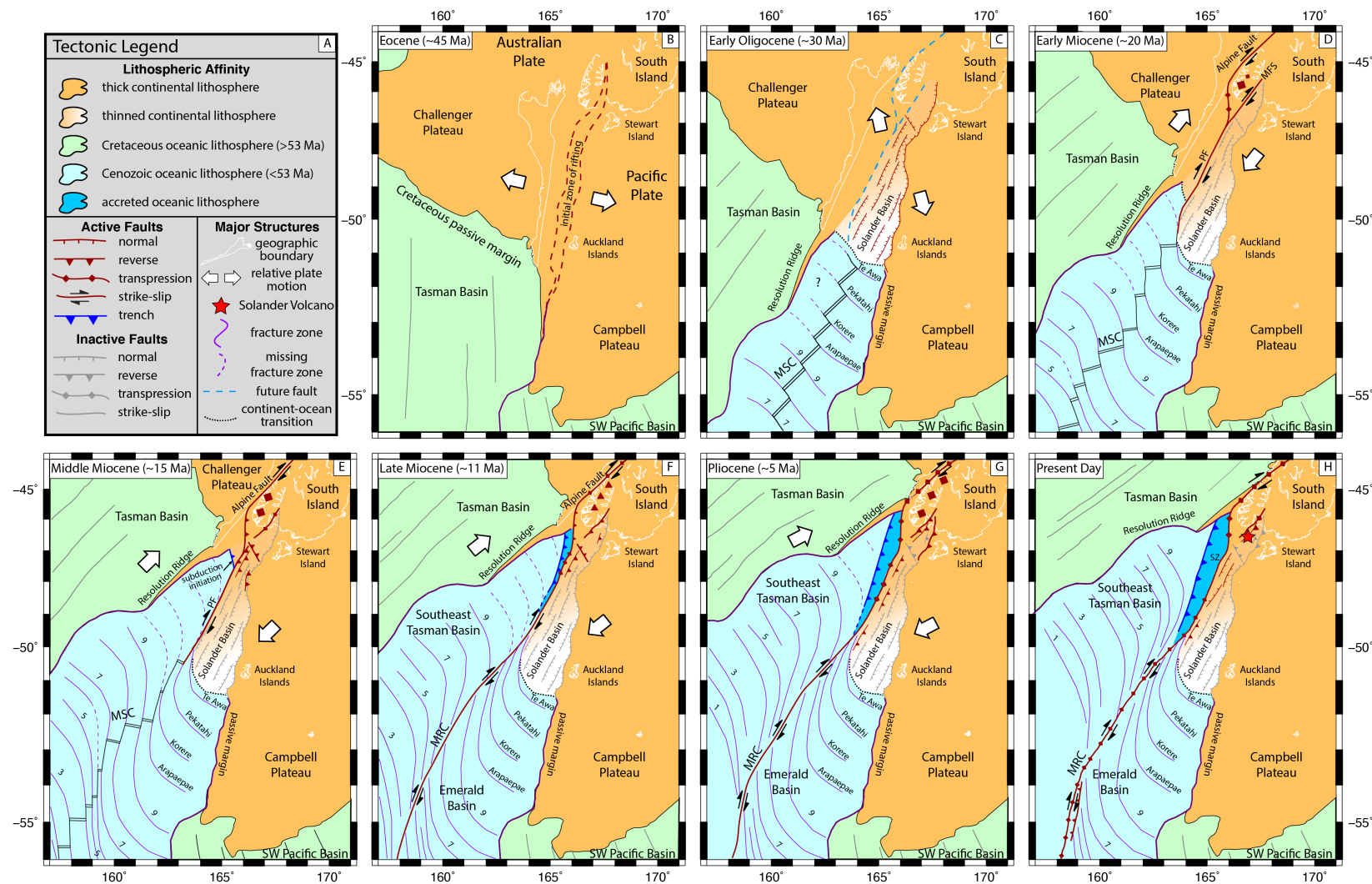


Figure 10. Interpreted map showing revised location of the Continent-Ocean Transition (COT) and oceanic sliver. Regional Bouguer gravity anomaly from GNS (<https://www.gns.cri.nz/Home/Products/Databases/New-Zealand-Region-Gravity-Grids; McCubbine et al., 2017>). Mafic gabbro, diabase, and basalt dredge samples shown in white stars from Mortimer (2014).

1340



1341

1342

1343

1344

1345

References

- Abers, G. A., Van Keken, P. E., Kneller, E. A., Ferris, A. & Stachnik, J. C. (2006). The thermal structure of subduction zones constrained by seismic imaging: Implications for slab dehydration and wedge flow. *Earth and Planetary Science Letters*, 241, 387-397. <https://doi.org/10.1016/j.epsl.2005.11.055>
- Axen, G. J., & Bartley, J. M. (1997). Implications for extensional tectonics. *Journal of Geophysical Research*, 102, 20,515-20,537. <https://doi.org/10.1029/97JB01355>
- Bache, F., Mortimer, N., Sutherland, R., Collot, J., Rouillard, P., Stagpoole, V., & Nicol, A. (2014). Seismic stratigraphic record of transition from Mesozoic subduction to continental breakup in the Zealandia sector of eastern Gondwana, *Gondwana Research*, 26(3-4), 1060-1078. <https://doi.org/10.1016/j.gr.2013.08.012>
- Bangs, N. L., Shipley, T. H., Gulick, S. P. S., Moore, G. F., Kuromoto, S., & Nakamura, Y. (2004). Evolution of the Nankai Trough décollement from the trench into the seismogenic zone: Inferences from three-dimensional seismic reflection imaging. *Geology*, 32, 273-276, <https://doi.org/10.1130/G20211.2>
- Beggs, J. M., Challis, G. A., & Cook, R. A. (1989). Basement geology of the Campbell Plateau: Implications for correlation of the Campbell Magnetic Anomaly System, *New Zealand Journal of Geology and Geophysics*, 33, 401-404. <https://doi.org/10.1080/00288306.1990.10425696>
- Bercovici, D., Ricard, Y., & Richards, M. A. (2003). The relation between mantle dynamics and plate tectonics: A primer. In M. A. Richards, R. G. Gordon and R. D. V. D. Hilst (Eds.), *The history and dynamics of global plate motions*, Geophysical Monograph Series (Vol. 121, pp. 5-46). Washington, DC: American Geophysical Union. <https://doi.org/10.1029/GM121p0005>
- Bishop, D. G., Bradshaw, J. D., & Landis, C. A. (1985). Provisional terrane map of South Island, New Zealand, in *Tectonostratigraphic terranes of the Circum-Pacific region*, Circum-Pacific Council for Energy and Mineral Resources earth science series 1: 515—521.
- Bown, J. W., & White, R. S. (1995). Effect of finite extension rate on melt generation at rifted continental margins, *Journal of Geophysical Research: Solid Earth*, 100(B9), 18011-18029. <https://doi.org/10.1029/94JB01478>
- Bradshaw, J. D. (1989). Cretaceous geotectonic patterns in the New Zealand Region, *Tectonics*, 8, 803-820. <https://doi.org/10.1029/TC008i004p00803>
- Butler, R. W. (2019). Syn-kinematic strata influence the structural evolution of emergent fold-thrust belts, *Geological Society of London Special Publications*, 490, SP490-2019. <https://doi.org/10.1144/SP490-2019-14>
- Cande, S. C., & Stock, J. M. (2004). Pacific-Antarctic-Australia motion and the formation of the Macquarie Plate. *Geophysical Journal International*, 157(1), 399-414. <https://doi.org/10.1111/j.1365-246X.2004.02224.x>
- Carpenter, B. M., Marone, C., & Saffer, D. M. (2011). Weakness of the San Andreas Fault revealed by samples from the active fault zone. *Nature Geoscience*, 4, 251-254, <https://doi.org/10.1038/ngeo1089>
- Chotalia, K., Cooper, G., Crameri, F., Domeier, M., Eakin, C., Grima, A. G., et al. (2020). The trans-disciplinary and community-driven subduction zone initiation (SZI) database, EGU General Assembly 2020, Online, 4–8 May 2020, EGU2020-15910, <https://doi.org/10.5194/egusphere-egu2020-15910>

- Christoffel, D. A., & Van der Linden, J. M. (1972). Macquarie Ridge - New Zealand Alpine Fault Transition, *Antarctic Research Series*. (Vol. 19). Washington, D.C: American Geophysical Union. <https://doi.org/10.1029/AR019p0235>
- Cloos, M. (1993). Lithospheric buoyancy and collisional orogenesis: Subduction of oceanic plateaus, continental margins, island arcs, spreading ridges, and seamounts, *Geological Society of America Bulletin*, 105(6), 715-737. [https://doi.org/10.1130/0016-7606\(1993\)105<0715:LBACOS>2.3.CO;2](https://doi.org/10.1130/0016-7606(1993)105<0715:LBACOS>2.3.CO;2)
- Coltice, N., Husson, L., Faccenna, C. & Arnould, M. (2019). What drives tectonic plates? *Science Advances*, 5, eaax4295, <https://doi.org/10.1126/sciadv.aax4295>
- Collot, J. Y., Lamarche, G., Wood, R. A., Delteil, J., Sosson, M., Lebrun, J. F., & Coffin, M. (1995). Morphostructure of an incipient subduction zone along a transform plate boundary: Puysegur Ridge and Trench. *Geology*, 23(6), 519–522. [https://doi.org/10.1130/0091-7613\(1995\)023<0519:MOAISZ>2.3.CO;2](https://doi.org/10.1130/0091-7613(1995)023<0519:MOAISZ>2.3.CO;2)
- Cooper, R. A. (1987). Early Paleozoic terranes of New Zealand, *New Zealand Journal of Geology and Geophysics*, 19, 73-112. <https://doi.org/10.1080/03036758.1989.10426457>
- Cox, S. C., & Sutherland, R. (2007). Regional geological framework of South Island, New Zealand, and its significance for understanding the active plate boundary. In D. Okaya, T. Stern, and F. Davey (Eds.), *A Continental Plate Boundary: Tectonics at South Island, New Zealand*, Geophysical Monograph Series (Vol. 175, pp. 19-46). Washington, DC: American Geophysics Union. <https://doi.org/10.1029/175GM03>
- Dalziel, I. W. D., & Dewey, J. F. (2019). The classic Wilson cycle revisited. In R. W. Wilson, G. A. Houseman, K. J. W. McCaffrey, A. G. Doré and S. J. H. Buiter (Eds.), *Fifty years of the Wilson cycle concept in plate tectonics*, Geological Society Special Publications (Vol. 470, pp. 19-38), London. <https://doi.org/10.1144/SP470.1>
- Davis, M., & Kusznir, N. (2002). Are buoyancy forces important during the formation of rifted margins? *Geophysical Journal International*, 149(2), 524-533, <https://doi.org/10.1046/j.1365-246X.2002.01666.x>
- Delteil, J., Collot, J. Y., Wood, R. A., Herzer, R., Calmant, S. Christoffel, D., et al. (1996). From strike-slip faulting to oblique subduction: A survey of the Alpine Fault-Puysegur Trench transition, New Zealand, results of cruise Geodyn-sud leg 2. *Marine Geophysical Researches*, 18, 383-399. <https://doi.org/10.1007/BF00286086>
- DeMets, C., Gordon, R. G., & Argus, D. F. (2010). Geologically current plate motions. *Geophysical Journal International*, 181, 1-80, <https://doi.org/10.1111/j.1365-246X.2009.04491.x>
- Dziewonski, A. M., Chou, T. -A., & Woodhouse, J. H. (1981). Determination of earthquake source parameters from waveform data for studies of global and regional seismicity. *Journal of Geophysical Research*, 86, 2825-2852. <https://doi.org/10.1029/JB086iB04p02825>
- Eberhart-Phillips, D., & Reyners, M. (2001). A complex, young subduction zone imaged by three-dimensional seismic velocity, Fiordland, New Zealand. *Geophysical Journal International*, 146, 731–746. <https://doi.org/10.1046/j.0956-540x.2001.01485.x>
- Eide, C. H., Schofield, N., Lecomte, I., Buckley, S., & Howell, J. A. (2018). Seismic interpretation of sill complexes in sedimentary basins: Implications for the sub-sill imaging problem. *Journal of the Geological Society of London*, 175, pp. 193-209. <https://doi.org/10.1144/jgs2017-096>

- 1437 Ekström, G., Nettles, M., & Dziewonski, A. M. (2012). The global CMT project 2004-2010:
1438 Centroid-moment tensors for 13,017 earthquakes. *Physics of the Earth and Planetary*
1439 *Interiors*, 200-201, 1-9. <https://doi.org/10.1016/j.pepi.2012.04.002>
- 1440 Fitch, T.J. (1972). Plate convergence, transcurrent faults, and internal deformation adjacent to
1441 southeast Asia and the western Pacific. *Journal of Geophysical research*, 77(23), pp.4432-
1442 4460. <https://doi.org/10.1029/JB077i023p04432>
- 1443 Frohlich, C., Coffin, M. F., Massell, C., Mann, P., Schuur, C. L., Davis, S. D., et al., (1997).
1444 Constraints on Macquarie Ridge tectonics provided by Harvard focal mechanisms and
1445 teleseismic earthquake locations. *Journal of Geophysical Research*, 102, 5029-5042,
1446 <https://doi.org/10.1029/96JB03408>
- 1447 Forsyth, D., & Uyeda, S. (1975). On the relative importance of the driving forces of plate
1448 motion. *Geophysical Journal of the Royal Astronomic Society*, 43(1), 163-200,
1449 <https://doi.org/10.1111/j.1365-246X.1975.tb00631.x>
- 1450 Gaina, C., Müller, D. R., Royer, J. Y., Stock, J., Hardebeck, J., & Symonds, P. (1998). The
1451 tectonic history of the Tasman Sea: a puzzle with 13 pieces. *Journal of Geophysical*
1452 *Research: Solid Earth*, 103(B6), 12413-12433. <https://doi.org/10.1029/98JB00386>
- 1453 Ghosh, A., & Holt, W. E. (2012). Plate motions and stresses from global dynamic models.
1454 *Science*, 335, 838-843. <https://doi.org/10.1126/science.1214209>
- 1455 Gradstein, F. M., Ogg, J. G., Schmitz, M. B., & Ogg, G. M. (Eds.). (2012). The geologic time
1456 scale 2012. Elsevier.
- 1457 Grobys, J. W. G., Gohl, K., & Eagles, G. (2008). Quantitative tectonic reconstructions of
1458 Zealandia based on crustal thickness estimates. *Geochemistry, Geophysics, Geosystems*,
1459 9(1), Q01005. <https://doi.org/10.1029/2007GC001691>
- 1460 Gurnis, M., Gulick, S. P. S., Stock, J., Van Avendonk, H. J. A., & Sutherland, R. (2019). Multi-
1461 Channel Seismic Shot Data from the Puysegur segment of the Macquarie Ridge Complex
1462 acquired during R/V Marcus G. Langseth expedition MGL1803 (2018). Integrated Earth
1463 Data Applications (IEDA). <https://doi.org/10.1594/IEDA/324659>
- 1464 Gurnis, M., Hall, C., & Lavier, L. (2004). Evolving force balance during incipient subduction.
1465 *Geochemistry, Geophysics, Geosystems*, 5(7), Q07001,
1466 <https://doi.org/10.1029/2003GC000681>
- 1467 Gurnis, M., Van Avendonk, H. J. A., Gulick, S. P. S., Stock, J., Sutherland, R., Hightower, E., et
1468 al. (2019). Incipient subduction at the contact with stretched continental crust: The Puysegur
1469 Trench. *Earth and Planetary Science Letters*, 520, 212-219.
1470 <https://doi.org/10.1016/j.epsl.2019.05.044>
- 1471 Hatherton, T. (1967). Total magnetic force measurements over the North Macquarie Ridge and
1472 Solander Trough, *New Zealand Journal of Geology and Geophysics*, 10(5), 1204-1211.
1473 <https://doi.org/10.1080/00288306.1967.10420211>
- 1474 Hayes, G. P., Furlong, K. P., & Ammon, C. J. (2009). Intraplate deformation adjacent to the
1475 Macquarie Ridge south of New Zealand-The tectonic evolution of a complex plate
1476 boundary. *Tectonophysics*, 463(1-4), 1-14. <https://doi.org/10.1016/j.tecto.2008.09.024>
- 1477 Heron, D.W. (2018). Geological map of New Zealand 1:250,000 (2nd ed Version 1). Lower
1478 Hutt, NZ: GNS Science. *GNS Science geological map 1* 1 USB stick.
- 1479 Hightower, E., Gurnis, M., van Avendonk, H. J. A., Stock, J., Gulick, S. P. S., & Sutherland, R.
1480 (2019). A 3D gravity inversion of the Puysegur Trench, New Zealand, with insights into
1481 subduction initiation, AGU Fall Meeting Abstract, T23C-0462.

- 1482 Holbrook, W. S., Purdy, G. M., Sheridan, R. E., Glover III, L., Talwani, M., Ewing, J., &
1483 Hutchinson, D. (1994). Seismic structure of the US Mid-Atlantic continental margin.
1484 *Journal of Geophysical Research: Solid Earth*, 99(B9), 17871-17891.
1485 <https://doi.org/10.1029/94JB00729>
- 1486 House, M. A., Gurnis, M., Kamp, P. J. J., & Sutherland, R. (2002). Uplift in the Fiordland
1487 region, New Zealand: Implications for incipient subduction. *Science*, 297(5589), 2038–
1488 2041. <https://doi.org/10.1126/science.1075328>
- 1489 Hunt International Petroleum Company. (1976). Well Completion Report Parara-1, Technical
1490 Report. Ministry of Economic Development.
- 1491 Kamp, P. J. (1986). The mid-Cenozoic Challenger Rift System of western New Zealand and its
1492 implications for the age of Alpine fault inception, *Geological Society of America Bulletin*,
1493 97(3), 255-281. [https://doi.org/10.1130/0016-7606\(1986\)97<255:TMCRSO>2.0.CO;2](https://doi.org/10.1130/0016-7606(1986)97<255:TMCRSO>2.0.CO;2)
- 1494 Karato, S.-I., & Barbot, S. (2018). Dynamics of fault motion and the origin of contrasting
1495 tectonic style between Earth and Venus. *Scientific Reports*, 8, 11884,
1496 <https://doi.org/10.1038/s41598-018-30174-6>
- 1497 Keller, W. R. (2004). *Cenozoic plate tectonic reconstructions and plate boundary processes in*
1498 *the Southwest Pacific*. Dissertation (PhD), California Institute of Technology, Pasadena,
1499 California. <https://doi.org/10.7907/VB6N-HC69>
- 1500 Klepeis, K. A., Webb, L. E., Blatchford, H. J., Jongens, R., Turnbull, R. E., & Schwartz, J. J.
1501 (2019). The age and origin of Miocene-Pliocene fault reactivations in the upper plate of an
1502 incipient subduction zone, Puysegur margin, New Zealand. *Tectonics*, 38(8), 3237–3260.
1503 <https://doi.org/10.1029/2019tc005674>
- 1504 Lachenbruch, A. H., & Sass, J. H. (1980). Heat flow and energetics of the San Andreas fault
1505 zone, *Journal of Geophysical Research*, 85, 6185–6222.
1506 <https://doi.org/10.1029/JB085iB11p06185>
- 1507 Laird, M. G., Bradshaw, J. D. (2004) The break-up of a long-term relationship: the Cretaceous
1508 separation of New Zealand from Gondwana, *Gondwana Research*, 7, 273-286.
1509 [https://doi.org/10.1016/S1342-937X\(05\)70325-7](https://doi.org/10.1016/S1342-937X(05)70325-7)
- 1510 Lamarche, G., & Lebrun, J.-F. (2000). Transition from strike-slip faulting to oblique subduction:
1511 active tectonics at the Puysegur Margin, South New Zealand. *Tectonophysics*, 316, 67–89.
1512 [https://doi.org/10.1016/S0040-1951\(99\)00232-2](https://doi.org/10.1016/S0040-1951(99)00232-2)
- 1513 Lamarche, G., Collot, J.-Y., Wood, R. A., Sosson, M., Sutherland, R., & Delteil, J. (1997). The
1514 Oligocene-Miocene Pacific-Australia plate boundary, south of New Zealand: Evolution
1515 from oceanic spreading to strike-slip faulting. *Earth and Planetary Science Letters*, 148(1–
1516 2), 129–139. [https://doi.org/10.1016/S0012-821X\(97\)00026-5](https://doi.org/10.1016/S0012-821X(97)00026-5)
- 1517 Lamb, S., Mortimer, N., Smith, E., & Turner, G. (2016). Focusing of relative plate motion at a
1518 continental transform fault: Cenozoic dextral displacement > 700 km on New Zealand's
1519 Alpine Fault, reversing > 225 km of Late Cretaceous sinistral motion, *Geochemistry*,
1520 *Geophysics*, *Geosystems*, 17(3), 1197-1213. <https://doi.org/10.1002/2015GC006225>
- 1521 Lebrun, J.-F., Lamarche, G., & Collot, J.-Y. (2003). Subduction initiation at a strike-slip plate
1522 boundary: The Cenozoic Pacific-Australian plate boundary, south of New Zealand. *Journal*
1523 *of Geophysical Research: Solid Earth*, 108(B9). <https://doi.org/10.1029/2002JB002041>
- 1524 Leng, W., & Gurnis, M. (2015). Subduction initiation at relic arcs, *Geophysical Research*
1525 *Letters*, 42, 7014-7021, <https://doi.org/10.1002/2015GL064985>
- 1526 Li, Z. X., Bogdanova, S. V., Collins, A. S., Davidson, A., De Waele, B., Ernst, R. E., et al.
1527 (2008), Assembly, configuration, and break-up history of Rodinia: A synthesis.

- Precambrian Research*, 160, 179-210, <https://doi.org/10.1016/j.precamres.2007.04.021>
- Lister, G. S., Etheridge, M. A., & Symonds, P. A. (1986). Detachment faulting and the evolution of passive continental margins. *Geology*, 14(3), 246–250. [https://doi.org/10.1130/0091-7613\(1986\)14<246:DFATEO>2.0.CO;2](https://doi.org/10.1130/0091-7613(1986)14<246:DFATEO>2.0.CO;2)
- Lithgow-Bertelloni, C., & Richards, M. A. (1995). Cenozoic plate driving forces, *Geophysical Research Letters*, 22, 1317-1320. <https://doi.org/10.1029/95GL01325>
- Martin, K., Gulick, S. P. S., Bangs, N., Moore, G., Ashi, J., Park, J.-O., et al. (2010). Possible strain partitioning structure between Kumano forearc basin and the slope of the Nankai Trough accretionary Prism: *Geochemistry, Geophysics, Geosystems*, 11, Q0AD02, <https://doi.org/10.1029/2009GC002668>
- Martin, K. M., Gulick, S. P. S., Austin, J. A., Berglar, K., Franke, D., Udrek, U., Permana, H. (2014). The West Andaman Fault: a complex strain-partitioning boundary at the seaward edge of the Aceh Basin, offshore Sumatra. *Tectonics*, 33, 786-806. <https://doi.org/10.1002/2013TC003475>
- Massell, C. G., Coffin, M. F., Mann, P., Mosher, S., Frohlich, C., Schuur, C. L., et al. (2000). Neotectonics of the Macquarie Ridge Complex, Australia-Pacific plate boundary. *Journal of Geophysical Research*, 105, 13,457-13,480. <https://doi.org/10.1029/1999JB900408>
- McCubbine, J. C., Stagpoole, V., Caratori Tontini, F., Amos, M., Smith, E., & Winefield, R. (2017). Gravity anomaly grids for the New Zealand region, *New Zealand Journal of Geology and Geophysics*, 60(4), 381-391. <https://doi.org/10.1080/00288306.2017.1346692>
- McDermott, K., & Reston, T. (2015). To see, or not to see? Rifted margin extension. *Geology*, 43(11), 967–970. <https://doi.org/10.1130/G36982.1>
- McIntosh, K., Lavier, L., van Avendonk, H. J. A., Lester, R., Eakin, D., & Liu, C. S. (2014). Crustal structure and inferred rifting processes in the northeast South China Sea. *Marine and Petroleum Geology*, 58(PB), 612–626. <https://doi.org/10.1016/j.marpetgeo.2014.03.012>
- McKenzie, D. P. (1977). The initiation of trenches: A finite amplitude instability. In M. Talwani and W. C. Pitman (Eds.), *Island arcs, deep sea trenches and back-arc basins*, AGU Maurice Ewing Series (Vol. 1, pp. 57-61). Washington, D.C. <https://doi.org/10.1029/ME001p0057>
- Meckel, T. A., Coffin, M. F., Mosher, S., Symonds, P., Bernardel, G., & Mann, P. (2003). Underthrusting at the Hjort Trench, Australian-Pacific plate boundary: Incipient subduction? *Geochemistry Geophysics Geosystems*, 4, 1099, <https://doi.org/10.1029/2002GC000498>
- Melhuish, A., Sutherland, R., Davey, F. J., & Lamarche, G. (1999). Crustal structure and neotectonics of the Puysegur oblique subduction zone, New Zealand. *Tectonophysics*, 313(4), 335–362. [https://doi.org/10.1016/S0040-1951\(99\)00212-7](https://doi.org/10.1016/S0040-1951(99)00212-7)
- Mortimer, N. (1994). Geological note: Igneous and sedimentary rocks dredged from the northern Macquarie Ridge, Southern Ocean. *AGSO Journal of Australian Geology and Geophysics*, 15, 529-537.
- Mortimer, N., Campbell, H. J., Tulloch, A. J., King, P. R., Stagpoole, V. M., Wood, R. A., et al. (2017). Zealandia: Earth's hidden Continent, *GSA Today*, 27, 27–35, <https://doi.org/10.1130/GSATG321A.1>
- Mortimer, N., Gans, P. B., Foley, F. V., Turner, M. B., Daczko, N., Robertson, M., & Turnbull, I. M. (2013). Geology and Age of Solander Volcano, Fiordland, New Zealand, *The Journal of Geology*, 121(5), 475-487. <https://doi.org/10.1086/671397>
- Mortimer, N., Gans, P. B., Meffre, S., Martin, C. E., Seton, M., Williams, S., et al. (2018). Regional volcanism of northern Zealandia: post-Gondwana break-up magmatism on an

- 1574 extended, submerged continent, *Geological Society of London Special Publications*, 463(1),
1575 199-226. <https://doi.org/10.1144/SP463.9>
- 1576 Mortimer, N., Tulloch, A. J., Spark, R. N., Walker, N. W., Ladley, E., Allibone, A., &
1577 Kimbrough, D. L. (1999). Overview of the Median Batholith, New Zealand: a new
1578 interpretation of the geology of the Median Tectonic Zone and adjacent rocks, *Journal of*
1579 *Asian Earth Sciences*, 29, 257-268, [https://doi.org/10.1016/S0899-5362\(99\)00095-0](https://doi.org/10.1016/S0899-5362(99)00095-0)
- 1580 Mueller, S., & Phillips, R. J. (1991). On the initiation of subduction. *Journal of Geophysical*
1581 *Research*, 96, 651-665. <https://doi.org/10.1029/90JB02237>
- 1582 Müller, R. D., Sdrolias, M., Gaina, C., & Roest, W. R. (2008). Age, spreading rates, and
1583 spreading asymmetry of the world's ocean crust, *Geochemistry Geophysics Geosystems*, 9,
1584 Q04006. <https://doi.org/10.1029/2007GC001743>
- 1585 Müller, R. D., Zahirovic, S., Williams, S., Cannon, J., Seton, M., Bower, D. J., et al. (2019). A
1586 global plate model including lithospheric deformation along major rifts and orogens since
1587 the Triassic, *Tectonics*, 38, 1884-1907. <https://doi.org/10.1029/2018TC005462>
- 1588 Nathan, S. (1976). Geochemistry of the Greenland Group (early Ordovician), New Zealand, *New*
1589 *Zealand Journal of Geology and Geophysics*, 19, 683-706.
1590 <https://doi.org/10.1080/00288306.1976.10426314>
- 1591 Norris, R. J., Carter, R. M., & Turnbull, I. M. (1978). Cainozoic sedimentation in basins adjacent
1592 to a major continental transform boundary in southern New Zealand. *Journal of the*
1593 *Geological Society*, 135, 191-205. <https://doi.org/10.1144/gsjgs.135.2.0191>
- 1594 Norris, R. J., & Turnbull, I. M. (1993). Cenozoic basins adjacent to an evolving transform plate
1595 boundary, southwest New Zealand. In P. F. Balance (Ed.), *South Pacific Sedimentary*
1596 *Basins of the World*, (Vol. 2, pp. 251-270). New York, NY: Elsevier.
- 1597 Osmundsen, P. T., & Ebbing, J. (2008). Styles of extension offshore mid-Norway and
1598 implications for mechanisms of crustal thinning at passive margins, *Tectonics*, 27, TC6016.
1599 <https://doi.org/10.1029/2007TC002242>
- 1600 Patel, J., Sutherland, R., Gurnis, M., Van Avendonk, H., Gulick, S., & Shuck, B. D. et al. (2020).
1601 Stratigraphic architecture of Solander Basin records Southern Ocean currents and
1602 subduction initiation beneath southwest New Zealand, *Basin Research*.
1603 <https://doi.org/10.1111/bre.12473>
- 1604 Raine, J. I., Beu, A. G., Boyes, A. F., Campbell, H. J., Cooper, R. A., Crampton, J. S., ... &
1605 Mortimer, N. (2015). New Zealand geological timescale NZGT 2015/1. *New Zealand*
1606 *Journal of Geology and Geophysics*, 58(4), 398-403.
1607 <https://doi.org/10.1080/00288306.2015.1086391>
- 1608 Reyners, M., Robinson, R., Pancha, A., & McGinty, P. (2002). Stresses and strains in a twisted
1609 subduction zone — Fiordland, New Zealand, *Geophysical Journal International*, 148, 637-
1610 648. <https://doi.org/10.1046/j.1365-246X.2002.01611.x>
- 1611 Riefstahl, F., Gohl, K., Davy, B., Hoernle, K., Mortimer, N., Timm, C., et al. (2020). Cretaceous
1612 intracontinental rifting at the southern Chatham Rise margin and initialisation of seafloor
1613 spreading between Zealandia and Antarctica. *Tectonophysics*, 776, 228298.
1614 <https://doi.org/10.1016/j.tecto.2019.228298>
- 1615 Rooney, T. O., Bastow, I. D., Keir, D., Mazzarini, F., Movsesian, E., Grosfils, E. B., et al.
1616 (2014). The protracted development of focused magmatic intrusion during continental
1617 rifting, *Tectonics*, 33, 875-897, <https://doi.org/10.1002/2013TC003514>
- 1618 Schofield, N., Holford, S., Millett, J., Brown, D., Jolley, D., Passey, S. R., ... & Hole, M. (2017).
1619 Regional magma plumbing and emplacement mechanisms of the Faroe-Shetland Sill

- 1620 Complex: implications for magma transport and petroleum systems within sedimentary
- 1621 basins, *Basin Research*, 29(1), 41-63. <https://doi.org/10.1111/bre.12164>
- 1622 Scott, J. M., Turnbull, I. M., Sagar, M. W., Tulloch, A. J., Waight, T. E., & Palin, J. M. (2015).
- 1623 Geology and geochronology of the Sub-Antarctic Snares Islands/Tini Heke, New Zealand,
- 1624 *New Zealand Journal of Geology and Geophysics*, 58, 202-212.
- 1625 <https://doi.org/10.1080/00288306.2015.1023810>
- 1626 Shillington, D. J., White, N., Minshull, T. A., Edwards, G. R. H., Jones, S. M., Edwards, R. A. &
- 1627 Scott, C. L. (2008). Cenozoic evolution of the eastern Black Sea: A test of depth-dependent
- 1628 stretching models, *Earth and Planetary Science Letters*, 265, 360-378.
- 1629 <https://doi.org/10.1016/j.epsl.2007.10.033>
- 1630 Stadler, G., Gurnis, M., Burstedde, C., Wilcox, L. C., Alisic, L. & Ghattas, O. (2010). The
- 1631 dynamics of plate tectonics and mantle flow: From local to global scales, *Science*, 329,
- 1632 1033-1038. <https://doi.org/10.1126/science.1191223>
- 1633 Stern, R. J. (2002). Subduction zones, *Reviews of Geophysics*, 40, 1012.
- 1634 <https://doi.org/10.1029/2001RG000108>
- 1635 Stern, R. J. (2004). Subduction initiation: spontaneous and induced, *Earth and Planetary Science*
- 1636 *Letters*, 226, 275-292. <https://doi.org/10.1016/j.epsl.2004.08.007>
- 1637 Stern, R. J., & Gerya, T. (2018). Subduction initiation in nature and models: A review.
- 1638 *Tectonophysics*, 746, 173-198. <https://doi.org/10.1016/j.tecto.2017.10.014>
- 1639 Sutherland, R. (1995). The Australia-Pacific boundary and Cenozoic plate motions in the SW
- 1640 Pacific: Some constraints from Geosat data, *Tectonics*, 14(4), 819-831.
- 1641 <https://doi.org/10.1029/95TC00930>
- 1642 Sutherland, R. (1999). Cenozoic bending of New Zealand basement terranes and Alpine Fault
- 1643 displacement: a brief review. *New Zealand Journal of Geology and Geophysics*, 42(2), 295-
- 1644 301. <https://doi.org/10.1080/00288306.1999.9514846>
- 1645 Sutherland, R., Gurnis, M., Kamp, P. J. J., & House, M. A. (2009). Regional exhumation history
- 1646 of brittle crust during subduction initiation, Fiordland, southwest New Zealand, and
- 1647 implications for thermochronologic sampling and analysis strategies. *Geosphere*, 5(5), 409–
- 1648 425. <https://doi.org/10.1130/ges00225.1>
- 1649 Sutherland, R., Davey, F., & Beavan, J. (2000). Plate boundary deformation in South Island,
- 1650 New Zealand, is related to inherited lithospheric structure. *Earth and Planetary Science*
- 1651 *Letters*, 177(3–4), 141–151. [https://doi.org/10.1016/S0012-821X\(00\)00043-1](https://doi.org/10.1016/S0012-821X(00)00043-1)
- 1652 Sutherland, R., & Melhuish, A. (2000). Formation and evolution of the Solander Basin,
- 1653 southwestern South Island, New Zealand, controlled by a major fault in continental crust
- 1654 and upper mantle. *Tectonics*, 19(1), 44–61. <https://doi.org/10.1029/1999TC900048>
- 1655 Sutherland, R., Barnes, P., & Uruski, C. (2006). Miocene-recent deformation, surface elevation,
- 1656 and volcanic intrusion of the overriding plate during subduction initiation, offshore southern
- 1657 Fiordland, Puysegur margin, southwest New Zealand. *New Zealand Journal of Geology and*
- 1658 *Geophysics*, 49(1), 131–149. <https://doi.org/10.1080/00288306.2006.9515154>
- 1659 Sutherland, R., Townend, J., Toy, V., Upton, P., Coussens, J. Allen, M., et al. (2017). Extreme
- 1660 hydrothermal conditions at an active plate-bounding fault, *Nature*, 546, 137-140,
- 1661 <https://doi.org/10.1038/nature22355>
- 1662 Sutherland, R., Dickens, G. R., Blum, P., Agnini, C., Alegret, L., Asatryan, G., et al. (2020).
- 1663 Continental-scale geographic change across Zealandia during Paleogene subduction
- 1664 initiation. *Geology*, 48, 419-424, <https://doi.org/10.1130/g47008.1>
- 1665 Thomson, K., & Hutton, D. (2004). Geometry and growth of sill complexes: insights using 3D

- 1666 seismic from the North Rockall Trough, *Bulletin of Volcanology*, 66(4), 364-375.
- 1667 <https://doi.org/10.1007/s00445-003-0320-z>
- 1668 Timm, C., Hoernle, K., Werner, R., Hauff, F., van den Bogaard, P., White, J., et al. (2010).
- 1669 Temporal and geochemical evolution of the Cenozoic intraplate volcanism of Zealandia,
- 1670 *Earth-Science Reviews*, 98(1-2), 38-64. <https://doi.org/10.1016/j.earscirev.2009.10.002>
- 1671 Toth, J., & Gurnis, M. (1998). Dynamics of subduction initiation at preexisting fault zones,
- 1672 *Journal of Geophysical Research*, 103, 18,053-018,068. <https://doi.org/10.1029/98JB01076>
- 1673 Tulloch, A. J., Ramezani, J., Mortimer, N., Mortensen, J., van den Bogaard, P., & Maas, R.
- 1674 (2009). Cretaceous felsic volcanism in New Zealand and Lord Howe Rise (Zealandia) as a
- 1675 precursor to final Gondwana break-up, *Geological Society of London Special Publications*,
- 1676 321, 89-118. <https://doi.org/10.1144/SP321.5>
- 1677 Turnbull, I. M., & Uruski, C. (1993). *Cretaceous and Cenozoic sedimentary basins of Western*
- 1678 *Southland*, South Island, New Zealand, Wellington, New Zealand: Institute of Geological &
- 1679 Nuclear Sciences Monograph.
- 1680 Uruski, C. I. (1992). Seismic evidence for dextral wrench faulting on the Moonlight Fault
- 1681 System, *Rec. N.Z. Geological Survey*, 44, 69-75.
- 1682 Van Avendonk, H. J., Shillington, D. J., Holbrook, W. S., & Hornbach, M. J. (2004). Inferring
- 1683 crustal structure in the Aleutian island arc from a sparse wide-angle seismic data
- 1684 set. *Geochemistry, Geophysics, Geosystems*, 5(8). <https://doi.org/10.1029/2003GC000664>
- 1685 Vissers, R. L. M., Drury, M. R., Strating, E. H. H., & van der Wal, D. (1991). Shear zones in the
- 1686 upper mantle: A case study in an Alpine Iherzolite massif, *Geology*, 19, 990-993,
- 1687 [https://doi.org/10.1130/0091-7613\(1991\)019<0990:SZITUM>2.3.CO;2](https://doi.org/10.1130/0091-7613(1991)019<0990:SZITUM>2.3.CO;2)
- 1688 White, R. S., Smith, L. K., Roberts, A. W., Christie, P. A. F., Kuszniir, N. J., Roberts, A. M., &
- 1689 the iSIMM Team (2008). Lower-crustal intrusion on the North Atlantic continental margin.
- 1690 *Nature*, 452(7186), 460-464. <https://doi.org/10.1038/nature06687>
- 1691 Wilson, J. T. (1966). Did the Atlantic Ocean close and then reopen? *Nature*, 211, 676-681.
- 1692 <https://doi.org/10.1038/211676a0>
- 1693 Wood, R., Lamarche, G., Herzer, R., Delteil, J., & Davy, B. (1996). Paleogene seafloor
- 1694 spreading in the southeast Tasman Sea, *Tectonics*, 15(5), 966-975.
- 1695 <https://doi.org/10.1029/96TC00129>
- 1696 Zhong, S., & Gurnis, M. (1996). Interaction of weak faults and non-Newtonian rheology
- 1697 produces plate tectonics in a 3D model of mantle flow, *Nature*, 383, 245-247.
- 1698 <https://doi.org/10.1038/383245a0>